Nanoscale

Cite this: *Nanoscale*, 2011, **3**, 2783

www.rsc.org/nanoscale

REVIEW

ZnO nanowire lasers

Daniël Vanmaekelbergh* and Lambert K. van Vugt†

Received 5th January 2011, Accepted 17th February 2011
DOI: 10.1039/c1nr00013f

The pathway towards the realization of optical solid-state lasers was gradual and slow. After Einstein's paper on absorption and stimulated emission of light in 1917 it took until 1960 for the first solid state laser device to see the light. Not much later, the first semiconductor laser was demonstrated and lasing in the near UV spectral range from ZnO was reported as early as 1966. The research on the optical properties of ZnO showed a remarkable revival since 1995 with the demonstration of room temperature lasing, which was further enhanced by the first report of lasing by a single nanowire in 2001. Since then, the research focussed increasingly on one-dimensional nanowires of ZnO. We start this review with a brief description of the opto-electronic properties of ZnO that are related to the wurtzite crystal structure. How these properties are modified by the nanowire geometry is discussed in the subsequent sections, in which we present the confined photon and/or polariton modes and how these can be investigated experimentally. Next, we review experimental studies of laser emission from single ZnO nanowires under different experimental conditions. We emphasize the special features resulting from the sub-wavelength dimensions by presenting our results on single ZnO nanowires lying on a substrate. At present, the mechanism of lasing in ZnO (nanowires) is the subject of a strong debate that is considered at the end of this review.

1. A brief history of ZnO lasing

In 1917 Einstein calculated the probabilities of absorption and stimulated emission of quanta from an electromagnetic beam.[1] The difference between the rates of absorption and stimulated emission, led to another process, *i.e.* the spontaneous emission of photons.[2] In stimulated emission, the probability of emission of a

Debye Institute for Nanomaterials Science, University of Utrecht, P.O. Box 80.000, 3508 TA Utrecht, The Netherlands. E-mail: d.vanmaekelbergh@uu.nl
† Current address: Department of Materials Science and Engineering, University of Pennsylvania, Philadelphia, Pennsylvania 19104, USA.

Daniël Vanmaekelbergh

Daniël Vanmaekelbergh was born in Bruges, Belgium in 1958 and obtained his PhD in chemistry from Ghent University in 1984. He joined Utrecht University in 1987, first as a postdoctoral researcher, later as assistant, associate and full professor. Currently he supervises the subgroup chemistry and physics of nanostructures in the condensed matter and interfaces group in the Debye Institute at Utrecht University. His research is focused on the optical and electronic properties of single, and assemblies of nanoparticles, using scanning probe microscopy and spectroscopy methods as well as well optical techniques.

Bert van Vugt

Bert van Vugt obtained his MSc in chemistry at Utrecht University with a thesis on non-aqueous electrodeposition of germanium for photonic crystal applications. After joining Daniël Vanmaekelbergh group at Utrecht University he obtained his PhD in chemistry in 2007 with a thesis on the optical properties of semiconducting nanowires. Later that year he joined Ritesh Agarwals group at the University of Pennsylvania as a postdoctoral fellow, where he studied and modeled nanowire waveguides, cavities and lasers. His current research interests include strong light-matter interaction at the nanoscale and nanoscale light sources.

photon of a given frequency is enhanced by the presence of another photon of the same frequency; the two photons then travel in phase and in the same direction. Hence stimulated emission leads to an increase in the number of photons travelling in phase in a certain direction (*i.e.* a coherent beam). The medium in which stimulation occurs is called the gain medium; it can be a gas of atoms, a liquid in which photoactive molecules are dissolved, or a semiconductor solid. Stimulated emission becomes possible in the case of population inversion, *i.e.* when the density of excited states is larger than that of the ground states. The energy to achieve this situation is delivered by photons absorbed in the gain medium or by electrical excitation. In the case of a semiconductor gain medium, the energy can be delivered by photons of energy above the optical laser transition, or, by electrical injection of charge carriers.

In order to enhance stimulated emission, the gain medium is placed in a cavity, *i.e.* a system with two mirrors in which the stimulation is made more efficient by back and forth travelling of the coherent electromagnetic beam. In the 1950's there was fierce competition between different research groups in the US and former Soviet Union working on a practical device that emits a coherent light beam by the process of stimulated emission. In 1959, the term LASER (light amplification by stimulated emission of radiation) was used for the first time in a scientific work. One year later, lasing at a 694 nm wavelength was demonstrated in ruby.[3–6] The first gas laser saw the light in the same year. This was followed in 1962 by the demonstration of an electrically driven (diode) laser based on GaAs (near IR).[7,8]

There was, hence, only a short time lapse between these landmarks and the first report in 1966 of lasing in the semiconductor ZnO with a band gap in the near UV.[9] A brief history of ZnO lasing is presented in Table 1, in which we present the year, and title of the publication, and some remarks. This table is based on the knowledge of the authors and the result of a search on the "ISI web of science", using *e.g.* "ZnO" + "laser" or "lasing" as keywords. We are aware that such an exercise does not lead to a complete list and might overlook important contributions, especially from the former Soviet Union. Even from a survey of only the titles it is clear that ZnO as a gain medium has its own special features. The excitations that lead to stimulated emission in a "normal" semiconductor are holes (empty electron levels at the top of the valence band) and electrons (filled levels at the bottom of the conduction band); the population inversion required for stimulated emission means that there are more occupied states at the bottom of the conduction band (*i.e.* conduction electrons) than empty states. Hence, the (quasi) Fermi level for electrons is situated in the conduction band and that for holes in the valence band. However, many reports on ZnO lasing emphasize that the fundamental excitation in ZnO lasing must be the exciton; an electron–hole artificial atom with discrete energy levels that is held together by the Coulomb attraction energy. Excitons hence have a lower energy than electron–hole pairs, and may be formed from electrons and holes spontaneously. In ZnO the electron–hole binding energy is particularly large (60 meV), *i.e.* more than twice the thermal energy at room temperature. This means that excitons are stable up to room temperature. Excitons and exciton–polaritons (see below) are important to understand the optical properties of ZnO at sufficiently low excitation intensity. Whether electrons and holes, or excitons are the elementary excitations responsible for ZnO lasing is a debate that is relevant up to this day, and will be discussed at the end of this review.

ZnO can be grown as macroscopic single crystals, thin (polycrystalline) films, quantum wells (electron confinement in one dimension), quantum rods (electron confinement in two dimensions), and quantum dots (electron confinement in three dimensions). Substantial electron confinement occurs if one or more of the dimensions becomes smaller than the exciton Bohr radius, about 3 nm (*vide infra*). One of the major reasons for the enormous scientific interest in ZnO is that all types of ZnO crystals show substantial luminescence (near the band gap in the near UV) and, in many cases, also stimulated emission and lasing. Hence, simple chemical growth methods may lead to functional opto-electronics in the near UV. The luminescence has been studied in detail, both in macroscopic ZnO crystals and in quantum-confined ZnO nanostructures. Concerning ZnO lasing, the mid 1990's showed a strong revival of scientific research with reports of lasing in macroscopic ZnO and polycrystalline thin films (see Table 1).

In 2001, room-temperature laser emission of ZnO nanowires was reported for the first time,[10] and this report led to a considerable focus of the research on the nanowire geometry. ZnO nanowires have diameters in the 100 nm range and do not show electronic confinement. There is, however, confinement of the electromagnetic waves in ZnO nanowires due to the dielectric contrast with the environment, leading to standing-wave electromagnetic modes. The considerable scientific interest in ZnO nanowires and the motivation for this review "ZnO nanowire lasers" has a number of reasons. First of all, wurtzite ZnO has a crystallographic polar axis (the *c*-axis) that is a natural axis of fast crystal growth. Hence several gas-phase and solution methods lead to ZnO crystals with an anisotropic 1-D shape (*i.e.* nanowire) with the polar *c*-axis as the long axis. The anisotropic crystals show hexagonal facets perpendicular to the *c*-axis. In many cases the "diameter" is between 100 and 500 nm, which is in the interesting range to support a limited number of quantized electromagnetic modes. These features lead to optical properties, not determined by the electronic energy levels of ZnO only, but also by the nanowire geometry. By knowing the exact relation between the lattice orientation and the nanowire geometry, analysis of polarized photoluminescence spectra gave a better microscopic understanding of the optical properties.[11] Moreover, ZnO nanowires show laser emission from the end-facets at room temperature.[12,13] A ZnO nanowire can hence be considered as one of the smallest possible room-temperature lasers together with hybrid plasmonic-semiconductor nanowire systems[252] and spasers.[253,260] The wire acts more or less as a natural cavity;[134] its sub-wavelength dimensions, however, lead to many new features, *e.g.* a reduced directionality of the emitted light beam.

2. Semiconductor nanowire lasers

In order to put the development of ZnO nanowire lasers into a more general framework of semiconductor nanowire opto-electronics we present a brief overview of the emergence of nanowire lasers in the scientific literature. Table 2, like Table 1, is based on the knowledge of the authors and a search on "ISI web

Table 1 Overview of publications on ZnO lasing. The table is based on the knowledge of the authors and a search on the web of science

Year	Title	Remarks	Ref.
1966	Ultraviolet laser pumped by an electron beam	Low temperature	9
1973	Exciton–exciton interaction and laser emission in high-purity ZnO		14
1996	Optically pumped ultraviolet lasing from ZnO		15
1997	Optically pumped lasing of ZnO at room temperature	Most cited landmark on lasing in macroscopic ZnO	16
1998	Room-temperature gain spectra and lasing in microcrystalline ZnO thin films		17
1998	Room-temperature ultraviolet laser emission from self-assembled ZnO microcrystallite thin films		18
1999	Photoluminescence and ultraviolet lasing of polycrystalline ZnO thin films prepared by the oxidation of the metallic ZnO	Extremely simple preparation of ZnO	19
2001	Room-temperature ultraviolet nanowire nanolasers	First report on the lasing of ZnO nanowires	10
2002	ZnO as a material mostly adapted for the realization of room-temperature polariton lasers	Emphasises exciton–photon coupling in ZnO nanostructures	20
2002	Room-temperature lasing observed from ZnO nanocolumns grown by aqueous solution temperature	Cheap, simple preparation	21
2003	ZnO *nanoribbon* microcavity lasers		22
2003	Soft-solution route to directionally grown ZnO nanorods arrays on Si wafer, room-temperature ultraviolet laser	Simple wet chemistry	
2003	Optical cavity effects in ZnO nanowire lasers and waveguides		23
2003	Dendritic *nanowire* ultraviolet laser array		24
2004	Ultrafast carrier dynamics in single ZnO *nanowire* and *nanoribbon* lasers		25
2004	Random laser action in ZnO nanorods arrays embedded in ZnO epilayers		26
2004	Whispering gallery modes in nanosized dielectric resonators with the hexagonal cross-section	Tapered ZnO wires	27
2004	Nanoribbon waveguides for subwavelength photonics integration	Lasing and guiding in long wires of ZnO, and SnO_2/ZnO links	28
2006	Phase-correlated non-directional laser emission from the end facets of a ZnO nanowire		13
2007	Excitonic ultraviolet lasing in ZnO-based light emitting devices	One of the first diode lasers	29
2007	Room-temperature stimulated emission of ZnO: alternatives to excitonic lasing		30
2008	Exciton–polariton formation at room temperature in a planar ZnO resonator structure		
2009	Random lasing in ZnO nanocrystals		31
2009	Imaging single ZnO vertical nanowire laser cavities using UV-laser scanning confocal microscopy		32

of science" with keywords "nanowire" + "laser or lasing". Interest in inorganic nanowire lasers started only at the beginning of this millennium, about two to three decades later than that for macroscopic semiconductor lasers. The citations on the material ZnO and its properties and functions grow in an exponential way, but that is not the case for nanowire lasing. Although one particular publication[10] received tremendous interest, as the first demonstration of a semiconductor nanowire laser, the scientific and technological interest in nanowire lasers is still moderate (if based on the number of citations) compared to that in nanowire growth and technology. This is remarkable considering the fact that the one-dimensional geometry may provide natural laser cavities and convenient contacting,[33] and the possibility to fabricate scanning AFM probes for (near field) optical excitation and collection.

The field of semiconductors for which (room temperature) nanowire lasing was demonstrated appears to be dominated by the II–VI materials, *i.e.* ZnO and CdS, while the only III–V material that is regularly reported in relation to nanowire lasing is GaN. All these semiconductors have a direct transition at the fundamental gap. The reason that lasing is observed in ZnO, CdS and GaN might be related to the exciton binding energy in these materials, which is considerably stronger than in other semiconductors, such as GaAs. In addition, III–V semiconductors show strong (surface) recombination[34–37] that could prevent the population inversion required for lasing. The first GaAs nanowire laser was only reported in 2009, and surface recombination is prevented by an ingenious co-axial core–shell structure.[38] It should be clear that besides the II–VI materials, also the III–V semiconductors, with direct band gaps extending in energy from the near IR to the near UV, and supported by a vast technological knowledge, also have a huge potential as the gain material for miniaturized nanowire lasers.

Only a limited number of groups provide mode calculations based on Maxwell theory or consider the microscopic physics.[11,39–44,254,255] We emphasize here that the optical physics of semiconductor nanowires is particularly rich due to the possible coupling of optical modes in the nanowire cavity with electron–hole excitations and excitons, resulting in optical properties that are determined not only by the electronic band gap of the material, but also by the nanowire geometry. Possibly, besides electrons and holes, and excitons coupled to electromagnetic modes, even more exotic electron–hole many-body correlations are important at low temperature and large excitation densities. We hope that this review on the optical properties of ZnO nanowires will lead to more interest of the physical community. Moreover, (ZnO) nanowire lasers and wave guides hold promise for novel applications in optical information

Table 2 Overview of the emerging field of semiconductor nanowire lasers. The table is based on the knowledge of the authors and a search on the web of science

Year	Title	Ref.	Comments
1993	Optical gain anisotropy in serpentine superlattice nanowire-array lasers	45	Organic nanowire
2001	Room-temperature ultra-violet nanowire lasers	10	First demonstration of nanowire lasing at room temperature
2001	Single nanowire lasers	46	
2002	Single GaN nanowire lasers	47	First III–V nanowire laser
2003	Single nanowire electrically driven lasers	33	First demonstration of an electrically driven nanowire laser, the semiconductor is CdS
2003	Reflection of guided modes in a semiconductor nanowire lasers	39	Modelling of the electromagnetic modes in a nanowire
2003	Optical cavity effects in ZnO nanowire lasers and waveguides	23	Idem
2004	Ultrafast carrier dynamics in single ZnO nanowire and nanoribbon lasers	25	Recombination dynamics
2004	Far-field emission of a semiconductor nanowire laser	41	Modeling: directionality of the emitted modes
2004	Modal gain in a semiconductor nanowire laser with optical bandstructure	40	Modeling of the gain for the different electromagnetic modes
2004	Whispering gallery modes in nanosized dielectric resonators with hexagonal cross-section	40	Calculation of modal gain for a wurtzite semiconductor wire with the *c*-axis being the long axis
2005	Bloch mode reflection and the lasing threshold in semiconductor nanowire laser arrays	42	Modeling of the mode propagation between the endfacets of a wire
2005	Lasing in single cadmium sulfide nanowire optical cavities	48	Evidence for lasing in CdS by exciton–exciton and exciton–phonon scattering
2005	Ultrafast wavelength-dependent lasing-time dynamics in single ZnO nanotetrapod and nanowire lasers	49	
2005	Semiconductor nanowire laser and nanowire waveguide electro-optic modulators	50	Modulation of lasing by an electric field
2005	GaN nanowire lasers with low lasing thresholds	51	
2005	Room-temperature nanowire ultraviolet lasers: an aqueous pathway for ZnO nanowires with low defect density	52	Cost effective fabrication of ZnO nanowires
2005	Low-order optical whispering-gallery modes in hexagonal nanocavities	53	
2006	Semiconductor nanowire ring resonator laser	54	First ring resonator based on a GaN nanowire
2006	Nanowire lasers with distributed-Bragg-reflector mirrors	55	
2006	Multiphoton route to ZnO nanowire lasers	56	Two-photon absorption converted into ultraviolet lasing
2006	Phase-correlated nondirectional laser emission from the end facets of a ZnO nanowire	13 and 57	Demonstration that lasing is non-directional *via* coherence effects
2007	Synthesis and lasing properties of highly ordered CdS nanowire arrays	58	
2007	Microstadium single-nanowire laser	59	
2008	Direct observation of whispering gallery modes and their dispersion in a ZnO tapered microcavity	60	
2008	Ultrafast upconversion probing of lasing dynamics in single ZnO nanowire lasers	61	Two-photon absorption converted into lasing
2008	Nanowire waveguides and ultraviolet lasers based on small organic molecules	62	
2008	Lasing dynamics in single ZnO nanorods	63	
2008	Whispering gallery mode lasing in ZnO microwires	64	
2009	The influence of local heating by non-linear pulsed laser excitation on the transmission characteristics of a ZnO nanowire wave guide	65	Heat modulation of laser emission
2009	Imaging single ZnO vertical nanowire laser cavities using UV-laser scanning confocal microscopy	32	
2009	Low-threshold two-photon pumped ZnO nanowire lasers	66	Two-photon absorption converted into lasing
2009	Refractive index dispersion deduced from lasing modes in ZnO microtetrapods	67	
2009	Lasing with guided modes in ZnO nanorods and nanowires	68	
2009	Polarization, microscopic origin, and mode structure of luminescence and lasing from single ZnO nanowires	11	Relates the polarization of the emission to the microscopic physics
2009	Single GaAs/GaAsP coaxial core–shell nanowire lasers	38	First nanowire laser based on GaAs
2009	Size-dependent waveguide dispersion in nanowire optical cavities: slowed light and dispersion less guiding	44	
2009	Nanowire photonics	256	Review including nanowire lasers
2009	Electrically driven ultraviolet lasing behavior from phosphorus-doped p-ZnO nanonail array/n-Si heterojunction	249	Electrically driven ZnO nanowire laser array
2010	Optically pumped nanowire lasers: invited review	69	
2010	Incorporating polaritonic effects in semiconductor nanowire waveguide dispersion	43	
2010	Semiconductor nanolasers	254	Tutorial on nanowire laser physics

processing and computing, and as local excitation sources in medical and biological research.

3. ZnO crystal lattice and electronic structure

The crystal structure and electronic structure of ZnO have been investigated extensively and reported in many research and review papers. Since the focus of this review is on nanowire lasers, we will only consider the most relevant points. For a more extensive review, we refer to Özgür.[70] The electronic configurations of the constituting atoms of the ZnO lattice are O: $1s^2\ 2s^2\ 2p^4$ and Zn: $1s^2\ 2s^2\ 2p^6\ 3s^2\ 3p^6\ 4s^2\ 3d^{10}$. Under normal conditions (*e.g.* atmospheric pressure), ZnO has a wurtzite crystal structure in which each Zn atom is coordinated to 4 O atoms as a tetrahedron, and *vice versa*. The ZnO bond is partly ionic; ZnO is often described as an ionic wurtzite lattice consisting of Zn^{2+} atoms (empty 4s orbital) and O^{2-} ions (completely filled 2p shell).

The wurtzite lattice is presented in Fig. 1; it can be described as two hcp lattices of the constituting atoms, interpenetrated in a layer-by-layer fashion. Related to this, one can consider a ZnO molecular unit aligned along the [0001] axis as a lattice point and check that the stapling of these points is ABAB, hence the molecular units also constitute a hcp lattice. This implies that the [0001] axis is a polar axis, referred to as the *c*-axis. Parallel to this *c*-axis, there are neutral planes that contain as many Zn as O atoms. The anisotropic crystal structure with the polar *c*-axis has important consequences for the chemistry of ZnO, *i.e.* growth and chemical etching, the electro-mechanical properties (piezoelectricity) and the opto-electronic properties. For instance, ZnO crystals grown by chemical vapor deposition on an oriented sapphire crystal grow as vertical wires (Fig. 1B); the fast growth direction is along the polar *c*-axis, the hexagonal symmetry with neutral lateral facets is evident from Fig. 1B.

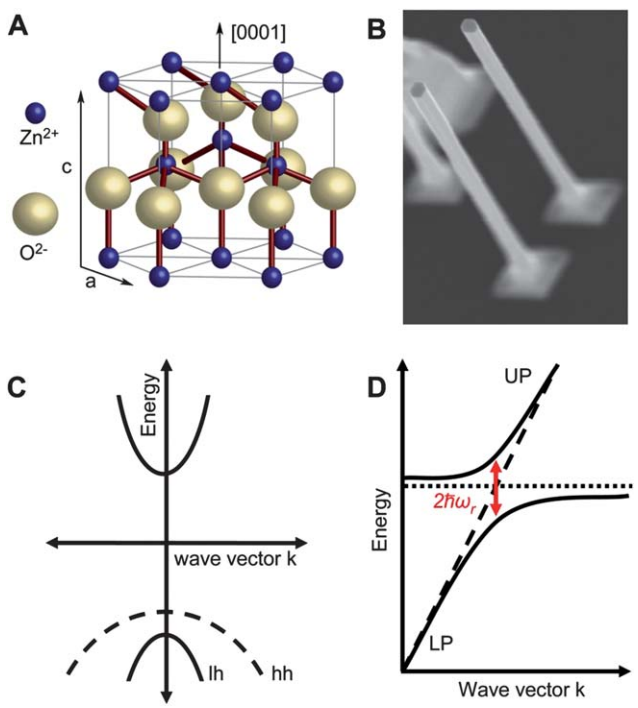

Fig. 1 The atomic and electronic structure, and the main optical excitations of ZnO in a nutshell. (A) Crystal structure with the polar *c*-axis in the vertical direction, (B) a ZnO nanowire on sapphire directed along the polar *c*-axis exhibiting a hexagonal crystal symmetry, (C) the basic electronic structure around the fundamental optical gap (Γ-point) with the light and heavy hole valence bands (lh and hh valence bands), (D) schematic energy *vs.* wave vector diagram of an exciton–polariton that arises from quantum mechanical interaction between the (B) exciton and a resonant photon. The arrow indicates the Rabi splitting, a measure of the strength of light–matter coupling.

The electronic structure (Fig. 1C) of the valence band of ZnO crystals has been investigated experimentally with angle-resolved photo-electron spectroscopy (ARPES). Theoretical work on the band structure of ZnO is based on pseudo-empirical methods (tight-binding and pseudo-potential calculations) as well as on first-principle studies. The electronic band structure related to the hcp lattices has a fundamental gap with a direct optical transition at the Γ point. The band gap is about 3.45 eV at 0 K, and about 3.37 eV at room temperature. The valence band is mainly related to the occupied 2p orbitals of the O^{2-} ions. Due to spin-orbit coupling and crystal field splitting, there are three valence-bands (heavy hole band, light hole band, and split-off band), each with a specific energy (E)–wave vector (k) relationship. This has important consequences for the optical properties as discussed below. The conduction band is related to the 4s orbitals of the Zn^{2+} ions.

With its large band gap with fundamental optical transition in the near UV, pure and undoped ZnO should be considered as a typical insulator. However, a ZnO crystal that is not intentionally doped is invariably an n-type semiconductor. The reason is that oxygen vacancies, interstitial Zn and interstitial H, present in the lattice of ZnO, constitute localised levels close to the conduction band, from which electrons can be excited into the band if the temperature is sufficiently high.[257] Since these species can be in chemical equilibrium with molecules such as oxygen and water absorbed at their surface, the degree of non-intentional doping in ZnO can vary depending on the conditions. This should always be taken in mind when electrical or optical results obtained with different experiments are compared. The influence of crystal impurities and defects on the optical properties at low-temperature is discussed below.

Intentional n-type doping has been obtained with trivalent atoms on the Zn position in the lattice, *e.g.* Al_{Zn}, Ga_{Zn}, In_{Zn}. However, for ZnO opto-electronic devices, such as electrically driven LEDs and LASERs, both p-type and n-type ZnO are required for the charge-injecting contacts. The quest for p-type doped ZnO is a long one. Publications on p-type ZnO started to appear in the beginning in this century,[71–75] and as for so many other topics related to the material ZnO, the research activity became extensive.[76–78] In the period 2005–2010, about 60 publications appeared each year. p-Type ZnO involves the controlled incorporation of impurity atoms in the lattice: As, Sb or P on an oxygen site, co-doping of Al or Ga and N, or group-I atoms on the Zn sites.[79,80] Although there are many reports on p-type conductivity in ZnO (nanowires), there is still considerable discussion on the reproducibility and robustness of the results, showing that p-type ZnO is not yet technologically mature. For a recent comprehensive review on the quest for p-type ZnO we refer the reader to ref. 258.

4. Optical excitations in macroscopic crystals of ZnO

4.1 Basic optical properties of ZnO

The optical properties of macroscopic ZnO crystals have been investigated extensively.[14,29,81–88] ZnO crystals can also be prepared with (one) of the dimensions so small (in the nanometre range) that the electron–hole excitations become quantum confined.[89–100] The optical transitions then increase in energy with decreasing dimensions. Typical ZnO nanowires have diameters in the 100 nm range, and show no quantum confinement of the electronic excitations. Their relevance lies in the confinement of the electromagnetic waves that are resonant with the optical transitions.

Nearly all ZnO specimens show bright luminescence when excited above the electronic band gap in the near UV; there is commonly a broad peak in the visible (the green peak), and a blue-near UV peak close to the band gap. The optical transitions of macroscopic single crystals have been investigated extensively using different types of optical spectroscopy, including angle-resolved, polarized photo-reflectance spectroscopy, absorption spectroscopy and photoluminescence spectroscopy. At cryogenic temperatures and low excitation energy there is a rich fine structure[101,102] due to (i) three excitonic transitions (A, B and C) related to the three valence bands,[103] (ii) excitons bound to various impurities, and (iii) coupling of excitons to the LO-phonon of the ZnO crystal (70 meV). The electron–hole binding energy of the excitons in ZnO is about 60 meV, which is remarkably strong compared to many other inorganic semiconductors. This large exciton binding energy together with the strength of the optical transitions make ZnO a material of huge interest for fundamental studies and applications.

At sufficiently high excitation intensity, the electron–hole attraction energy is strongly screened, and the main excitations are (weakly correlated) electrons and holes (electron–hole plasma). It is obvious that the transition between the exciton regime and the regime of electron–hole plasma must be gradual. It is however often indicated as the Mott transition density;[104,105] the carrier density needed to screen the electron–hole attraction energy is about 5×10^{18} cm^{-3}.

For the present review, with its focus on room-temperature lasing in ZnO nanowires, the free excitons are of importance. At 5 K, the A, B and C excitons are located at 3.37, 3.4 and 3.44 eV, respectively. With increasing temperature, the resonances become broader (damping) and also shift to lower energy, the latter is due to the temperature-dependent lattice affecting the electronic band gap. The B and C excitonic optical transitions have the strongest oscillator strength. The transition dipole moment of the A and B excitons is oriented perpendicular to the polar *c*-axis whereas the C exciton has its transition dipole moment oriented parallel to the *c*-axis. These features are essential in understanding the optical properties of ZnO nanowires as will be discussed below.

Fig. 2 (curves a and b) shows the room-temperature luminescence spectrum under low-intensity xenon lamp excitation, measured for a sample with ZnO nanowires grown vertical on a sapphire substrate (Fig. 2, right panels). There is a broad luminescence peak in the green, due to defect-related emission,

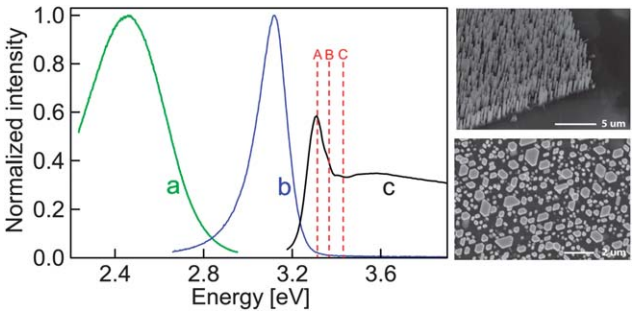

Fig. 2 Basic optical properties of ZnO nanowires at room temperature. Spectra a and b show the photoluminescence spectra of ZnO nanowires grown on sapphire (see also Section 5) as shown in the SEM pictures on the right. Spectrum c is a photoluminescence excitation spectrum for luminescence monitored in the green. The marked peak reflects the generation of excitons at room temperature. The fine structure is related to the A, B and C excitons, which are partly resolved.

and a peak in the near UV-blue region, very similar to what is commonly observed for macroscopic ZnO crystals of a high crystalline quality. A detailed investigation with strongly quantum-confined nanocrystals provided evidence that the green emission is due to a transition between a defect state (oxygen vacancy) located in the gap and (one of) the valence bands.[98] More information on the green transition, obtained by polarized luminescence spectroscopy with single nanowires is presented below. The ratio of the green intensity with respect to the interband emission depends on the quality of the sample and on conditions such as humidity and excitation intensity. The photoluminescence excitation spectrum (acquired at room temperature by monitoring the green emission) shows a marked peak, which cannot be described by the onset of band gap absorption and the generation of free carriers. Instead, the peak provides a clear signature of A, B and C excitonic transitions at room temperature. The orientation of the transition dipole moment is different for the three optical transitions: A and B excitons have their transition dipole moment oriented perpendicular to the polar *c*-axis of the ZnO crystal; this means that the wave vector *k* of the resonant photons can still be oriented perpendicular to the *c*-axis (named σ polarization) or parallel to the *c*-axis (named α polarization).[87] The C-exciton has its transition dipole moment parallel to the *c*-axis, and hence the wavevector *k* is perpendicular to the *c*-axis. It is clear that the orientation of the transition dipole moment is important for the quantum mechanical coupling between the electron–hole exciton and its resonant electromagnetic wave in the nanowire cavity.

4.2 Exciton–polaritons in macroscopic crystals of ZnO

In a simple view, one could state that due to their high electron–hole binding energy and strong oscillator strength, excitons are the primary excitations in ZnO crystals in a wide range of temperature and at sufficiently low excitation intensity. There is, however, an important physical phenomenon that should be discussed here that makes this picture physically more accurate and helps to understand the optical properties of ZnO micro- and nanostructures. In the sixties, Hopfield and Thomas were the first to consider the quantum mechanical interaction of a photon

travelling in a semiconductor crystal with its resonant electron–hole exciton.[106–108] Their argument is that both limiting states can convert into each other in a coherent way as long as nothing irreversible happens. Quantum-mechanically, the travelling photon and the resonant exciton can be considered as two states that interact, leading to an avoided crossing in the energy–wavevector dispersion and two new composite particles, *i.e.* exciton–polaritons.[20,60,84,85,87,109–128] The new quasi-particles are represented in the energy *vs.* wave-vector dispersion by the lower and upper polariton branch, respectively. There is a similarity with the bonding and anti-bonding molecular levels that arise from the interaction of resonant orbitals of two atoms. The energy gap between the two levels is also known as the normal-mode splitting or Rabi-splitting, a measure of the strength of the exciton–photon interaction. For instance, the energy-level splitting in the semiconductor GaAs is about 0.1 meV.[125,129] This splitting can be considerably enhanced in cavities with standing-wave photon states, with GaAs as the active material. In macroscopic ZnO, the splitting determined with angle-resolved reflection spectroscopy is about 10 meV.[20,112,130] This is about a factor of hundred larger than in GaAs, and can be considered as a sign of extremely strong light–matter interaction. Hence, the optical properties of macroscopic ZnO at sufficiently low temperature and excitation density are, in fact, best understood with the picture of exciton–polaritons, not excitons. In nanostructures of ZnO however,[20,131] light–matter interaction is even much stronger than in macroscopic crystals. This means that at sufficiently low excitation intensity exciton–polaritons govern the properties of ZnO nanostructures, even up to room temperature. Exciton–polaritons, having partly a photon-like character can be described by Maxwell's equations, and thus also with the resulting wave-equation:

$$\nabla^2\vec{E} - \mu_0\varepsilon_0(\omega)\frac{\partial^2\vec{E}}{\partial t^2} = 0 \qquad (1)$$

Harmonic plane waves with an electric field vector $\vec{E} = \vec{E}_0 e^{i(\vec{k}\vec{r}-\omega t)}$ are solutions of this equation. Substitution gives the relationship between the wave vector $\vec{k}$and the frequency ω of the exciton–polariton travelling in an isotropic nonmagnetic semiconductor characterised by the dielectric function $\varepsilon(\omega,\vec{k})$. Hence, the energy levels of the exciton–polariton branches are given by:

$$\vec{E}(\omega,\vec{k}) = \hbar\omega = \frac{\hbar c\vec{k}}{\sqrt{\varepsilon(\omega)}} \qquad (2)$$

One can see that the relationship between the wave vector and frequency differs from that of an electromagnetic wave in vacuum by the factor $1/\sqrt{\varepsilon(\omega)}$. Hence the dielectric function $\varepsilon(\omega)$ determines the energy–wave vector dispersion relation of exciton–polaritons. In principle, $\varepsilon(\omega)$ can be calculated on the basis of a microscopic model. However, it has been shown that the macroscopic Lorentz model for a damped oscillator can be used in practice. The dielectric function is then given by:

$$\varepsilon(\omega) = \varepsilon_b\left(1 + \frac{Ne^2}{\varepsilon_b m_e}\frac{f}{\omega_0^2 - \omega^2 - i\omega\gamma}\right) \qquad (3)$$

where ω_0 = transverse exciton frequency, γ = the damping constant, N the number of atomic oscillators per unit volume with an oscillator strength f. The oscillator strength, $0 < f < 1$, expresses the relative strength of a given transition from a well defined ground state, with respect to the sum of the strengths of all transitions from that same ground state. The oscillator strength can be related to the longitudinal–transverse splitting of an optical transition that can be directly obtained from reflection spectroscopy.[112,130] For vanishing damping one obtains:

$$f\frac{Ne^2}{\varepsilon_b m_e} = \omega_L^2 - \omega_T^2 \qquad (4)$$

The transverse resonance frequency ω_T is in fact close to the resonance frequency ω_0 at which the dielectric function increases steeply to infinity (see eqn (3)). The longitudinal frequency ω_L is the frequency for which the dielectric function becomes zero. Substitution of eqn (4) into (3), and combining this equation with eqn (2), gives a useful expression for the exciton–polariton energy levels close to an exciton resonance:

$$E(\omega,\vec{k}) = \hbar\omega(\vec{k}) = \frac{\hbar c\vec{k}}{\sqrt{\varepsilon_b\left(1 + \frac{\omega_L^2 - \omega_T^2}{\omega_T^2 - \omega^2 - i\omega\gamma}\right)}} \qquad (5a)$$

Eqn (5a) provides the energy levels of the upper and lower branches of a propagating exciton–polariton, as a function of its wave vector $\vec{k}$. Essential factors are the number and strength of the oscillators and their damping. Plots of the exciton polariton equation for increasing longitudinal–transverse splitting are presented in Fig. 3, in which the damping has been neglected. It can be seen that the splitting becomes larger for increasing fN. This type of calculation, applied to the three exciton resonances A, B and C, agrees reasonably well with the optical results obtained with macroscopic ZnO crystals and thin films. We emphasize that this macroscopic modelling can only be a first step in understanding the optical properties. There are currently strong efforts being made to understand the optical properties of ZnO on the basis of a microscopic first-principle model that does not make *a priori* assumptions on the existence of excitons and exciton–polaritons.[132]

However, it will become clear that with ZnO nanowires the splitting between the polariton branches can be much larger than that calculated above.[11,121,131,133] The polariton—eqn (5a)—can still be used to understand the photoluminescence spectrum and the lasing spectrum under the condition that the longitudinal–transverse splitting in eqn (5a) is enhanced considerably with

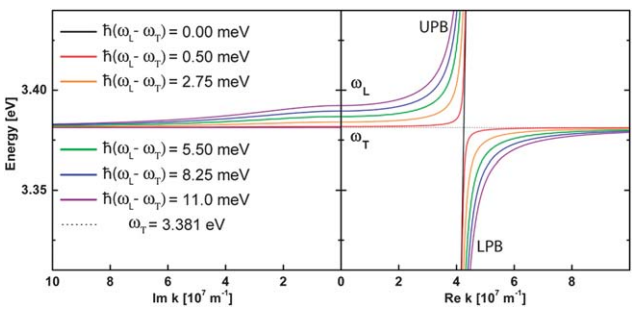

Fig. 3 The polariton energy levels in ZnO, for increasing longitudinal–transverse splitting (a measure for the coupling strength) calculated with eqn (5a). The calculation is especially relevant for the B and C exciton resonances in a macroscopic crystal of ZnO which show splittings in the range of 10 meV.

respect to that measured with bulk crystals. Hence, in ZnO nanostructures, the effects of light–matter interaction are dramatically stronger than in macroscopic crystals. This has been anticipated in a visionary paper.[20] The strong light–matter interaction in ZnO nanostructures and ZnO nanowires leads to a size and shape dependence of the optical properties of the nanostructures, and can hence be tailored by materials engineering.

4.3. ZnO under strong optical excitation

A microscopic first-principle theory for ZnO under optical excitation has just been developed.[132] Under intense excitation of the dielectric, the electron–hole attraction energy becomes significantly screened by excitons themselves and, more effectively, by electrons and holes. The electron–hole binding energy weakens, and excitons are split into independent or weakly correlated electrons and holes. In addition, the band gap of ZnO reduces markedly in magnitude with increasing density of electrons and holes. It should be clear that although the optical properties of ZnO are governed by excitons at sufficiently low (cryogenic) temperature and/or excitation intensity, this is not necessarily the case at higher densities and temperatures. Whether room temperature ZnO lasing is mediated by exciton–polaritons or electrons and holes is a topic of strong debate, as discussed below.

5. The growth of ZnO nanowires

Synthesis methods of ZnO nanowires and nanorods can be roughly divided into solution and vapour phase methods. Solution phase synthesis generally encompasses low temperature electrochemical,[135] chemical[136] and hydrothermal[137] routes. In the higher temperature vapour phase synthesis, a distinction with regard to the source of Zn and O atoms can be made. From low to high temperature, vapour-phase synthesis precursors can be produced by: metallo-organics,[138] laser ablation of ZnO,[139–141] thermal evaporation of zinc metal in the presence of (an) air/O_2 (plasma),[142–144] carbo-thermal reduction of ZnO leading to the formation of zinc vapor and carbon oxides[145–152] and direct thermal evaporation of ZnO.[153–155] Lower temperature methods have the advantages of greater substrate compatibility and limited interdiffusion between substrate and wire whereas the higher temperature vapor phase methods generally provide higher crystallinity, orientation, and better optical and electronic properties due to annealing effects. In principle, these synthesis methods can be combined with patterning and templating[156] and epitaxial methods to obtain positional control, directed growth and integrated functionality such as contacts or p/n junctions.

Wurztite ZnO has good epitaxial compatibility with sapphire (Al_2O_3), GaN, InP and of course ZnO. The ZnO unit cell *a*-axis (3.296 Å) is related to the sapphire unit cell *c*-axis (12.99 Å) by a factor of four resulting in the epitaxial configuration of ZnO (0001)[110]||sapphire(110)[0001] with a lattice mismatch of only 0.08% at room temperature.[157] On wurztite GaN with lattice parameters $a = 3.189$ Å and $c = 5.185$ Å the epitaxial relation is ZnO(0001)[110]||GaN(0001)[110] with a lattice mismatch of 1.9%[158] and there is also evidence for the epitaxial growth of *c*-axis oriented ZnO on the (100) InP surface.[141,159] Epitaxial growth on technologically important Si substrates has only been achieved using buffer layers.[160]

Vapor phase growth can be achieved with or without (metal) catalyst particles: the catalyst route is known as Vapor–Liquid–Solid (VLS) growth,[145,161,162] the catalyst-free route as Vapor–Solid (VS) growth,[163,164] a hybrid of these two growth mechanisms has also been reported (see further).[156] The VLS mechanism consists of three stages. First, a metal particle absorbs semiconductor material and forms an alloy. In this step the volume of the particle increases and the particle often shows a solid/liquid phase transition. Second, the alloy particle absorbs more semiconductor material until it is saturated. The saturated alloy droplet attains equilibrium with the solid phase of the semiconductor and nucleation occurs (*i.e.* solute/solid phase transition). During the final phase, a steady state is formed in which a semiconductor crystal grows at the solid/liquid interface. The precipitated semiconductor material grows as a wire because it is energetically more favorable to extend the wire's side faces rather than extend the solid–liquid interface.[165] An advantage of growth *via* the VLS mechanism is that the wire diameter is determined by the diameter of the alloy particle which is in turn determined by the size of the initial metal particle and the temperature. The nanowire length is simply determined by the growth time. Direct control over the nanowire geometry can hence be obtained by controlling the initial catalyst particle size, temperature and growth time.[166] Disadvantages include left over metallic conducting particles on the substrate that can disrupt conduction patterns and serve as light scattering sources, metal doping of the nanowires and the inevitable metallic particles at the tip of the nanowires that can serve as efficient scattering sources for light confined in the nanowire cavity, making VLS grown wires less desirable for lasing applications. In fact, to our knowledge no studies have been published in which a nanowire which had an integrated catalyst particle from VLS growth showed stimulated emission, although an *ex situ* deposited aluminium layer on the end facet provided a higher reflectivity as evidenced by a lower lasing threshold and cavity *Q*-factor.[167]

Growth according to the VS mechanism utilizes the natural tendency of ZnO crystals to grow along the crystallographic *c*-axis ([0001] direction), favouring expansion of the lower energy neutral $(10\bar{1}0)$ planes over enlargement of the higher energy polar (0001) plane. Evidence for two detailed VS growth mechanisms involving either sequential nucleation and growth steps of pyramids on the (0001) plane and subsequent fast growth of the pyramid [1123] faces[163] or a continuous layer by layer growth on the 0001 top face[138,164] has been put forward. VS growth results in wurtzite nanowires grown along the *c*-axis, with hexagonal cross-sections and without integrated catalyst particles. This makes VS growth the preferred method to obtain ZnO nanowire laser cavities since the absence of catalyst particle results in laser cavities of high morphological, optical and electronic quality. The wire's aspect ratio is determined by the different growth rates of the (0001) end face and the $\{10\bar{1}0\}$ side faces resulting typically in nanowires with diameters in the 100–300 nm range and lengths of several tens of micrometres. Using VS growth, stimulated emission has been obtained in ZnO nanowires grown using carbo-thermal reduction,[150–152] laser ablation,[140] metallo

organics,[138] evaporation of zinc[142–144,168] and evaporation of ZnO.[153–155]

Most of the results highlighted in this review were obtained on ZnO nanowires grown epitaxially on polished a-plane sapphire substrates by the carbo-thermal reduction of ZnO by graphite powder at 880 °C for 30 min in an argon flow, using a plasma sputter coated gold layer of 7 Å. After growth, the substrates were examined using X-ray diffraction and scanning electron microscope imaging (see *e.g.* Fig. 2). The diffractogram was dominated by a single peak which could be indexed to the (0002) plane of the ZnO wurztite crystal structure with cell parameters $a = 3.24$ Å and $c = 5.19$ Å, indicating preferred c-axis orientation. Top and side views of Scanning Electron Microscopy (SEM) images of the growth substrate confirmed that the wires of ~10 microns and 200–300 nm diameter grew as single crystals epitaxially along the c-axis as evidenced by the hexagonal cross-sections and the orientation of the nanowire crystal side faces. The wires only grew in the gold deposition area, but curiously enough, gold catalyst particles of typically an order of magnitude smaller dimensions than the nanowire cross-sections, could only be observed at the substrate side of the nanowires, not at the tips. This provides evidence for a hybrid VLS–VS growth mechanism in which the gold nanoparticles act as initial nucleation/collection sites, after which VS growth takes over.[156] The absence of catalyst particles on the tips of the nanowires in many ZnO nanowire lasing studies that used catalyst particles to grow,[146–149,169] points to the importance of this hybrid growth mechanism for obtaining stimulated emission from ZnO nanowires.

6. Confined photon and exciton–polariton modes in ZnO nanowires

One-dimensional single crystals of ZnO can be grown in a wide variety of diameters between 1 nm and 1 μm (see Section 5). In view of the optical properties, thinner and thicker ZnO nanowires should be distinguished. The optical transitions of ZnO are at around 3.3 eV; the corresponding wavelength of the resonant electromagnetic mode is thus $\lambda = hc/nE$, (n is the refractive index of ZnO), which is about 125 nm. An electromagnetic mode can be supported in the nanowire if the half-wavelength (65 nm) fits the lateral dimension. Hence we should consider ZnO *nanorods* that have a diameter (considerably) smaller than 65 nm, and *nanowires* with a diameter above 65 nm.

In ZnO nanorods (diameter < 65 nm), the optical polarizability is much larger along the long axis: thin nanorods will absorb and emit light with the electric field oriented preferentially along the long axis. This can be understood on the basis of electrostatic arguments solely. Experimental support for linearly polarized absorption and emission in thin semiconductor rods has been presented recently.[170–172]

If the diameter of the ZnO nanowire becomes larger than 65 nm, a transverse electromagnetic mode iso-energetic with the (exciton) transition can be guided (see Fig. 4) due to the dielectric contrast of the ZnO crystal with its environment. In other words, such ZnO nanowires act as resonators and waveguides for modes that have a wave vector parallel to the long axis, which is nearly always the c-axis of the wire. If the diameter of the ZnO nanowires increases further, new transverse modes appear.

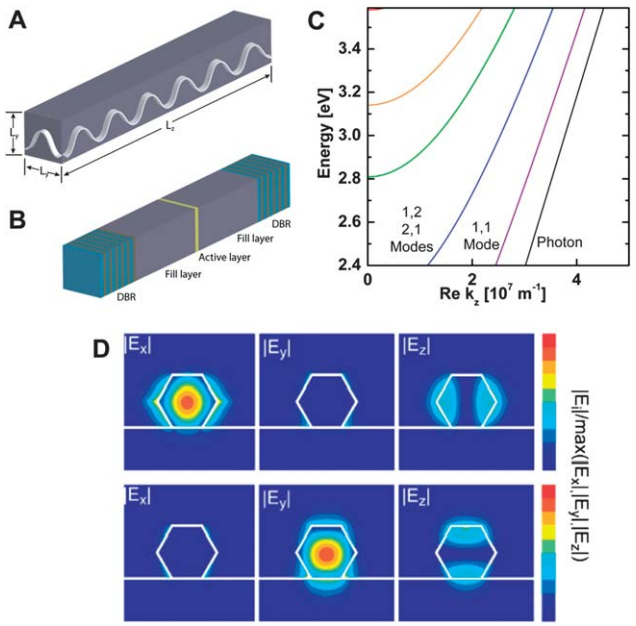

Fig. 4 Models for electromagnetic photon and polariton modes in a ZnO nanowire. Top: schematics for purely photonic electromagnetic modes in a (tetragonal) nanowire. (A) Wave picture of the mode for which the half-wavelength fits in the short direction. Panel (B) demonstrates how mode-reflection at the end-facets can be improved by Bragg reflectors. (C) Photon energy levels for lateral confined photonic modes, as a function of the wavevector k_z in the long direction of the wire (|| c-axis) assuming a perfect electrical conductor nanowire surface boundary. Bottom, (D) the field intensities in the x, y and z direction for the two degenerate lowest order HE_{11} modes localized between the two end-facets of a hexagonal wire with 86 nm edges; the modes are nearly linearly polarized ⊥ c-axis (with k_z || c-axis) *i.e.* nearly TE modes.

Whispering gallery modes become possible for diameters above 500 nm.[53,60,64,173]

Due to the large oscillator strength of the exciton transitions in ZnO, the exciton and electromagnetic modes strongly interact which leads to an upper and lower exciton–polariton branch as shown in Fig. 5. Li *et al.* calculated the exciton–polariton mode structure for the experimental situation of a ZnO nanowire with hexagonal symmetry lying on a silica substrate.[11] The calculation is based on the solution of Maxwell's equations with a finite

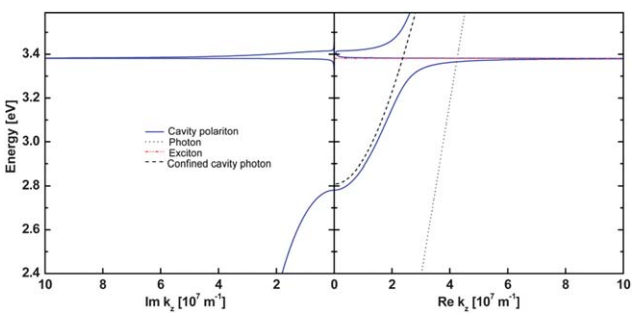

Fig. 5 Dispersion relation for exciton–polariton modes laterally confined in a long ZnO nanowire (tetragonal geometry), the quantum numbers $m_x = m_y = 1$, while m_z can vary freely. The longitudinal–transverse splitting of the B-exciton has been chosen on the basis of measurements on bulk ZnO, *i.e.* 11 meV. The exciton resonance is at 3.381 eV and a damping of 0.11 meV was used.

element method and the dielectric function is given by the Lorentz model (eqn (3)). Fig. 4 presents the simplest lowest order modes (HE_{11}, linearly polarized) with colour plots of the amplitude of the electric field in the lateral directions $|E_x|$ and $|E_y|$, and the long-axis $|E_z|$. This representation is chosen in order to show the polarization and confinement of the modes. It is clear that the modes spill over the edges of the nanowire, and that the silica substrate has a disturbing influence by sucking away the intensity of the mode with the linear polarization vertical to the substrate. The consequences of this for optical collection in the far field are discussed below.

Assuming a perfect conducting nanowire surface, the energy levels of purely photonic and exciton–polariton modes can be discussed on the basis of eqn (5a) as expressed by:

$$E(k_x, k_y, k_z) = \frac{\hbar c}{\sqrt{\varepsilon(\omega)}}\sqrt{k_x^2 + k_y^2 + k_z^2} \quad (5b)$$

Results are displayed in Fig. 5. If the dielectric function $\varepsilon(\omega)$ is reduced to the dielectric constant ε_b, the modes become purely photonic. This is a good approximation for energies considerably below the exciton transitions or at excitation densities above the Mott transition where free or weakly correlated electrons and holes determine the optical properties. The components of the wave vector of the confined modes in a nanowire with perfect conducting surfaces are given by:

$$k_{x,y,z} = m_{x,y,z}\frac{\pi}{L_{x,y,z}} \quad (6)$$

The quantum numbers m_x and m_y define the energy cut off at $k_z = 0$ (Fig. 4). The photonic energy levels increase dramatically with increasing lateral quantum number m_x (m_y), and the allowed quantum numbers are low (usually 1 or 2). In the long direction, much larger quantum numbers are possible. For sufficiently long wires the energy levels form a quasi-continuum as a function of the wave vector in the long direction, k_z for each pair (m_x, m_y) (Fig. 4). For short wires (typically below 20 μm) the energy levels with different m_z become distinguishable in optical experiments in the far field (see below).

The coupling of the photonic modes to the excitons changes the mode dispersion relation especially in the energy range close to the exciton transitions due to the fast change of $\varepsilon(\omega)$. The energy level scheme calculated with eqn (5b) is given in Fig. 5 (for a sufficiently long wire, with closely spaced energy levels).

The most significant effect is the avoided crossing between the confined photon line (dashed) and the resonant exciton energy level, this gives rise to the upper and lower confined polariton branch (blue lines in Fig. 5). Experiments with ZnO nanowires[121] show a larger splitting of the upper and lower polariton branch, than that observed with macroscopic crystals.[112] Hence, the effect of exciton–photon coupling appears to be more pronounced in certain nanostructures than in macroscopic crystals.

7. Optical properties of ZnO nanowires

7.1 The optical properties of ZnO nanowires have been studied from different perspectives

Research on the optical properties of ZnO nanowires (and nanorods) started in the beginning of this millennium, and is rapidly expanding. The optical properties of ZnO nanowires have been studied for different reasons: (i) the first motivation is a standard optical characterization of as-prepared arrays of ZnO nanowires.[124,174–193] It has been presented in Section 5 that ZnO nanowires can be grown by a plethora of different methods, from room-temperature electrodeposition and chemical-bath deposition to high temperature (1100 °C) gas-phase deposition. The wires vary strongly in quality and defect density. A standard characterization involves measurement of the photoluminescence spectrum of an array of nanowires. There is a remarkable consistency in the *qualitative* features of ZnO luminescence, with a broad luminescence peak in the green spectral range and near-band gap luminescence at around 3.3 eV. In general, ZnO nanowires prepared at low-temperature show relatively more defect emission and possibly more non-radiative recombination than wires grown with high temperature methods. A typical result acquired on an array of ZnO nanowires grown with CVD at high temperature is presented in Fig. 2. Arrays of ZnO nanowires grown and contacted with cost-effective low-temperature methods hold promise for large-scale electrically driven lighting and photovoltaics. (ii) There are a relatively large number of publications that report the cathodoluminescence of *single* ZnO nanowires.[23,194–198] The Cathodo-Luminescence (CL) is measured in a Scanning Electron Microscope (SEM), such that a direct relation between the light emission and the nanowire geometry can be obtained. The excitation spot interaction volume (~50 nm) is small with respect to both diameter and length of the nanowire studied, so that the effect of nanowire geometry, lattice strain, and local excitation (waveguiding) on the optical properties can be monitored (see below), although to our knowledge stimulated emission in ZnO nanowires has not been obtained by electron beam pumping. (iii) The third motivation to study the optical properties of ZnO nanowires is to understand the origin and nature of the guided photonic modes, which play such an important role in luminescence and lasing.[11,60,121,133,199] The studies deal with single ZnO nanowires of known geometry; wires are locally excited, or in other cases the luminescence is detected in a local way using a pinhole in the objective plane of the microscope or by near-field optical microscopy. With these spectroscopic methods, the guided photonic modes have been detected and analyzed. Several studies report remarkable results on "sub-wavelength" mode guiding in single wires and basic photonic structures important for applications, while other studies aim to understand the nature and origin of the guided modes (see Section 7.2). The following section will deal with a thorough characterization of the guided modes. (iv) Study of electrically driven emission using n-type ZnO in a hetero-system, or a ZnO nanowire p–n junction.[97,183,199–214,249] ZnO nanowires have an easy geometry for electrical contacts and hold promise for electrically driven light emission in miniaturized LEDs and LASERS. These applications will be discussed at the end of this review in Section 11.

Below, we review the work performed with local excitation or local detection on single wires standing perpendicular or lying parallel to the substrate. This work aims to characterize the guided modes in ZnO. It will become clear that, *at sufficiently low excitation intensity*, these modes are influenced by light–matter interaction, and can be described as exciton–polariton modes. At higher excitation intensity, some of the modes develop into

a laser mode. The different viewpoints on the nature of these modes, *i.e.* exciton–polaritonic or arising from an electron–hole plasma will be discussed in Section 10.

7.2 Detection of the upper and lower polariton branch by measurement of the single-wire luminescence with a scanned excitation spot

As has been discussed above, the optical properties will be determined by exciton–polaritons if the exciton–photon coupling is sufficiently strong. We recall that in the case of macroscopic ZnO crystals the polariton branches have been measured with angle-resolved reflection spectroscopy. The excitation of well-defined exciton–polaritons, of given energy and wave vector, is reflected in the (sharp) absorption resonances of a monochromatic light beam incident on the ZnO surface at varying angle.[84,112,130] In this way, it was observed that the normal mode splitting between the upper and lower branch is about 5 meV; this large value points to strong light–matter interaction in macroscopic crystals of ZnO.

The question that we wish to resolve now is how the upper and lower polariton branches (*i.e.* the energy levels) can be studied experimentally in the geometry of a nanowire. It is impossible to measure the absorbed intensity from the reflection, since there will be strong light scattering in all directions. A direct measurement of the upper and lower polariton branches from the luminescence spectrum itself[87,109] does not provide a clear (E,k) dispersion relation of the upper branch, since the luminescence from the upper branch has low intensity, possibly due to the fast decay to the lower branch. In principle, the upper branch could be characterized by photoluminescence-excitation spectroscopy, monitoring the luminescence in the lower branch when the excitation energy is scanned through the energy range of the upper branch.[108] This experiment has not yet been reported.

We have chosen to map the upper and lower branch of single ZnO nanowires in a rather unusual way by scanning the excitation spot (two-photon energy above the upper branch) along the total length of the wire and measuring the wire's luminescence spectrum.[121] The work is performed with a pulsed laser, and is based on frequency doubling in the ZnO nanowire, leading to excitation at 3.54 eV. The scanning excitation spot—single wire luminescence—is based on the principle that the luminescence intensity $I(\hbar\omega_{em})$ reflects the relative probability of excitation of a number of modes in the energy-window of the detector $\hbar\omega_{em} \pm \Delta$ (Δ being 5 meV). This probability of exciting modes in a given energy range is higher at the wire ends, since there the different modes have their field amplitudes all with the same sign, while at the center of the wire the modes have a random orientation of the field with respect to each other. Hence the enhancement factor $F(\hbar\omega_{em} \pm \Delta) = I(\hbar\omega_{em}^{\text{end excitation}})/I(\hbar\omega_{em}^{\text{center excitation}})$ reflects the mode density, *i.e.*, at $E = \hbar\omega_{em} \pm \Delta$ in the wire. For limited ranges of the emitted photon energy, it was observed that the total wire emission was strongly enhanced when the excitation spot was located at a wire end (Fig. 6). Trivial effects such as a better in-coupling of the excitation light at the wire ends could be excluded. First of all, this enhancement is only observed for limited energy regions. For instance, the frequency-doubled emission below the exciton energy remained constant if the excitation spot is scanned, ruling out the possibility of more efficient incoupling at the wire ends (not shown in Fig. 6). Further evidence came from measuring the cathodo-luminescence of the ZnO wire: when the exciting electron beam was scanned along the wire, it was again found that the modes of certain energy were much more intense if the beam was exciting the wire ends. The luminescence of a single wire and the enhancement factor of a given wire are plotted in Fig. 6. The enhancement factor shows a striking spectral dependence, with two peaks, separated by a gap. The peaks indicate the high mode density pertaining to the flattened regions of the dispersion curve of the upper and lower branches close to the exciton resonance(s) (see Fig. 5). Hence, the gap between the two peaks should reflect the Rabi-splitting between the branches. Depending on the wire, splittings between 60 and 160 meV were observed, showing that exciton–photon coupling is much stronger in nanowires than in macroscopic ZnO crystals. This strong light–matter interaction has been predicted from theoretical arguments.[20,131] At higher excitation intensities, the peaks in the enhancement spectrum disappear gradually, due to the disappearance of the excitons in favor of free or weakly correlated electrons and holes. This last result forms another strong indication that the peaks in the enhancement spectrum reflect the upper and lower polariton branch.[215] The light emission of (tapered) vertical nanowires has also been characterized by ingenious optical spectroscopy and related to the existence of exciton–polaritons.[60,216] We note here that the optical properties of planar resonator structures of ZnO have been studied in detail.[123,217]

7.3 ZnO nanowires show three distinct luminescence regimes

ZnO nanowires show a bright luminescence in the visible and the near UV. The ratio of the defect to UV luminescence depends on the quality of the ZnO crystal and the excitation intensity. The quality of the ZnO nanowires that we have grown at high temperature is very high, and the UV luminescence dominates over the defect emission, except for very low excitation intensities (see Fig. 3). In order to understand the nature of the luminescence of single ZnO nanowires we performed spectroscopy on single wires lying on a silicon or silicon nitride substrate. The

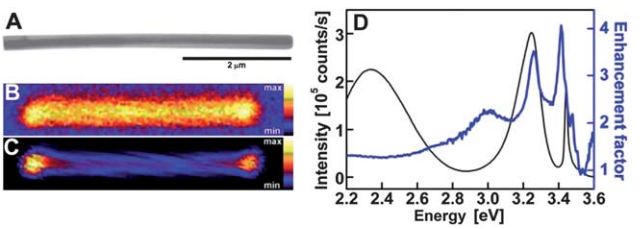

Fig. 6 Scanning non-resonant excitation spectroscopy of a single ZnO nanowire. The wire (length 5 μm, radius about 200 nm) lies on a silicon-nitride substrate. Top left: SEM picture of the wire and colour representation of the local excitation probability of green defect luminescence (top) and near band-gap polariton emission (bottom). Right: black line: luminescence spectrum of the wire excited with the light of 1.77 eV *via* second harmonic generation showing the green defect luminescence, the polariton luminescence (peak between 3 and 3.4 eV), and the second harmonic light (3.54 eV) that was not absorbed in the wire. Blue spectrum: the enhancement factor (see text) as a function of the energy of the emitted photons. The two sharp peaks indicate the high mode density of the lower and upper polariton branch.

wires are uniformly excited, and the luminescence was acquired in a spatially resolved way using a pinhole in the image plane of the microscope. In a second study, a polarizer was also used in order to detect the polarization of the emitted light. We remark here that measuring the polarization of a wire lying on a substrate is not trivial; experimental details on the accuracy of the polarization detection can be found in ref. 11. In this review the results at room temperature are most important and will be discussed. A comprehensive picture of the luminescence of two single ZnO nanowires is presented in Fig. 7. With regard to the spatial pattern of the emitted light, three different regimes of light emission could be distinguished.

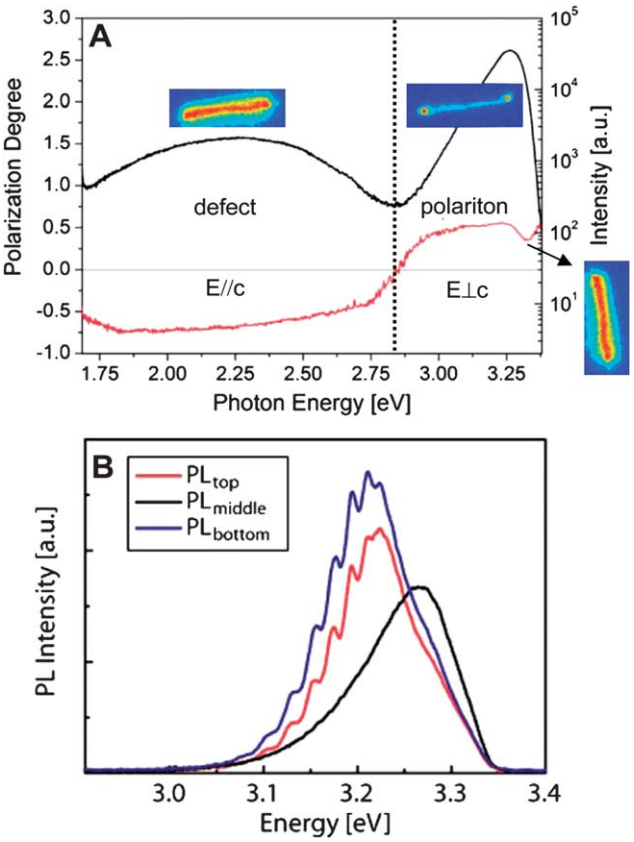

Fig. 7 Spatially and polarization resolved photoluminescence spectroscopy on single ZnO nanowires. (A) Photoluminescence spectrum (black line) and the degree of polarization of the emitted light (red line); the spatial dependence of the emission along the wire is also shown (ZnO nanowire, length = 12 μm, diameter = 250 nm, excited with a 349 nm laser). Three different regimes of emission can be detected: (i) defect luminescence between 1.75 and 2.9 eV, uniformly emitted along the wire with the electric field ∥ wire axis (= *c*-axis), (ii) between 2.9 and 3.22 eV, exciton–polariton emission from the wire ends (*k* ∥ wire axis, field vector ⊥ wire axis), (iii) a third contribution peaked at 3.3 eV uniformly emitted along the wire with the field vector ⊥ wire axis). (B) Spatially resolved luminescence spectrum between 2.9 and 3.4 eV: the emission spectrum at both wire ends is identical and shows Fabry–Pérot modes super-imposed on a background; the emission spectrum acquired at the center of the wire shows enhanced emission around 3.3 eV, uniformly emitted along the wire (ZnO nanowire, length = 4.9 μm, diameter = 200 nm, excited with a 349 nm laser, 2.3 W cm^{-2}).

The first regime involves a broad spectrum mainly in the visible between 1.7 and 2.9 eV where light emission is due to recombination *via* a defect state in the band gap. The light is uniformly emitted along the entire length of the wire and is, strikingly, also considerably polarized with the electric field vector parallel to the wire length (*c*-axis). The polarization indicates that the C-exciton (heavy hole valence band) must be involved. A study of the defect luminescence of ZnO quantum dots showed that the defect luminescence is due to recombination of a trapped electron (very probably in an oxygen vacancy) with a valence hole.[218] The dominant polarization, field parallel to *c*-axis, can then be explained by recombination of the trapped electron with a hole in the heavy-hole C valence band.

The second regime, between 2.9 and 3.25 eV, is characterized by luminescence from both wire ends. This means that guided modes are detected, with the wave vector *k* parallel, and the electric field vector perpendicular to the *c*-axis (long axis). We detected a polarization $E \perp c$-axis and also nearly parallel to the substrate. This preferential polarization can be explained by the linearly polarized modes discussed in Section 6, with the addition that the linearly polarized mode with orthogonal polarization is strongly absorbed in the substrate. The spatially resolved detection is presented in Fig. 7, bottom panel. Both wire ends show identical spectra, with a series of Fabry–Pérot modes, indicating that they are delocalized between the end-facets of the wire. The modes of a given nanowire are not equidistant in energy, the spacings become smaller with increasing wave vector. In Fig. 9, the Fabry–Pérot modes are plotted in the energy–wave vector diagram. It can be seen that the energy–wave vector plot is strongly curved, and can be fitted with the polariton equation [eqn (5a)] provided that the normal mode splitting is enhanced by a factor of 5. Hence, these results can be understood in terms of very strong exciton–photon coupling, in a similar way as the excitation results presented above. The evolution of the exciton–polariton modes with increasing excitation intensity will be discussed in the next session.

Now, we discuss the third regime of light emission at around 3.3 eV. We note that this third regime emerges most clearly from the abrupt change of emission from the wire ends ($\hbar\omega_{em} < 2.26$ eV) to uniform wire emission ($\hbar\omega_{em} \geq 2.26$ eV) and simultaneously a marked change in the polarization (Fig. 7A). Due to its polarization dependence, the emission in this regime has been attributed to the C-exciton or to (weakly correlated) electron–hole pairs.

8. Studies of lasing in ZnO nanowires

A brief history of ZnO (nanowire) lasing was given in Sections 1 and 2. The first paper that showed lasing from an (ordered) array of vertical ZnO nanowires grown on a sapphire substrate was published in 2001, and got enormous attention.[10] This was followed by publications that reproduced the room-temperature lasing in ZnO nanowire arrays and single wires that stand up or lie on a substrate. Detailed studies of the laser emission and its dynamics followed. The optical excitation used consisted of direct supra band gap excitation, or was based on intense nano-second or pico-second pulses of sub-band gap light, the carriers being excited by frequency doubling or tripling. In addition, the dynamics of lasing have been measured with pump-probe

spectroscopy. There is an interesting discussion on the mechanism of lasing.

In 2003, Yan *et al.* reported laser emission from ZnO nanowires grown out of a ZnO ribbon to form a comb.[24] In 2003, Johnson *et al.* also reported a detailed characterization of room-temperature lasing from ZnO nanowires.[23] He described stimulated emission of modes with k parallel to the wire's long axis (c-axis) as well as laser emission in the perpendicular direction. This agrees with a later study in 2009 by Li *et al.* who observed that the laser modes are guided ($E \perp c$, $k \parallel c$) but that thicker wires also show laser modes with opposite polarization ($E \parallel c$).[11] The latter indicates whispering gallery modes. In 2006, van Vugt *et al.* reported the lasing from single wires lying on a substrate.[13] The interference pattern that formed at the onset of lasing indicated coherence as well as guided modes emitted in a non-directional way. In 2009, Gargas *et al.* reported a detailed study of a vertical ZnO laser cavity using scanning confocal microscopy in the UV.[32]

The laser dynamics were first studied by Johnson *et al.* in 2004,[25] and later by Song *et al.* in 2005.[49] The dynamics of a single ZnO nanowire laser also characterized by SEM were reported in 2008 by Fallert *et al.*[63] Laser emission arising from sub-band gap excitation and frequency doubling or tripling was studied by Zhang *et al.* in 2006,[56] and by Song *et al.* in 2008.[61]

9. From luminescence to lasing

We have examined the evolution from luminescence to lasing for single ZnO nanowires lying flat on a silica substrate using a luminescence microscope.[13] A typical result is presented in Fig. 8. It should be remembered that ZnO nanowires show three regimes of luminescence, which could be distinguished by the energy and polarization of the emitted photons, and the position at which the photons leave the nanowire. The second regime, *i.e.* the exciton–polariton luminescence regime, is highlighted in Fig. 8, two upper panels. It is characterized by a series of Fabry–Pérot modes emitted from the end facets. It was reported that these luminescence modes increase in a supra-linear way with the excitation intensity, *i.e.* $I(k_z) \propto I_{ex}^n$ with n between 1.6 and 1.9.[133] This strongly indicates that the luminescence arises from polariton–polariton scattering. When the excitation intensity is enhanced to 139 W cm^{-2}, the second highest energy mode (at 3.19 eV) sharpens considerably and gains height, *i.e.* is converted into a lasing mode (bottom-left). At an excitation intensity of 268 W cm^{-2}, this mode and its neighbor form dominant lasing modes. At the onset of lasing, the CCD image of the emitting wire abruptly shows a pronounced interference pattern. This interference pattern is explained as the result of emission of each photon at both ends of the nanowire; the lasing modes have a phase difference of 0 or π. Hence, lasing from both ends of the nanowire shows a strong similarity to the famous two-slit experiment of Young. The interference pattern also implies that the modes are not emitted in a forward direction, but in an almost spherical fashion.

Maslov and Ning calculated the laser emission from a semiconductor nanowire characterized by a passive dielectric constant.[41] Nanowires with a sufficiently large radius can support the hybrid-electric, transverse-electric and transverse-magnetic modes. Strikingly, the emission of these modes in the length

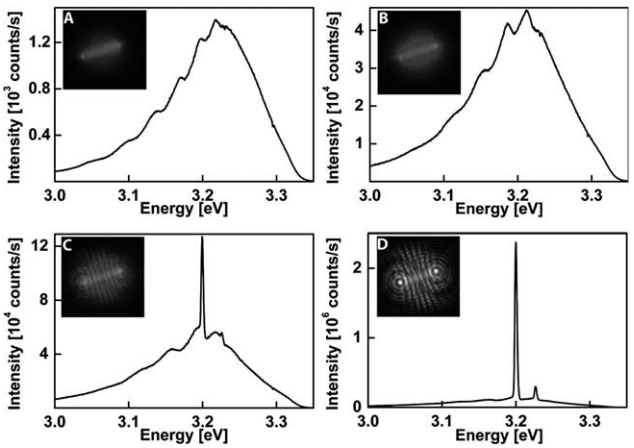

Fig. 8 Evolution from luminescence to lasing of a single ZnO nanowire (about 200 nm in diameter, 3 μm in length) lying on a silica substrate, excited with a 350 nm pulsed laser. Top-left: luminescence spectrum at an excitation power of 24 W cm^{-2}, top-right: luminescence spectrum at an excitation power of 93 W cm^{-2} with the onset of lasing, bottom-left: spectrum at an excitation power of 139 W cm^{-2} with one mature lasing peak, bottom-right: luminescence spectrum at an excitation power of 268 W cm^{-2} with two mature lasing peaks. The onset of lasing is also visible by the interference patterns recorded with a CCD.

directions (forward and backward) of the nanowire was zero, but non-zero over all other angles with respect to the nanowire axis, *i.e.* an approximately spherical emission pattern. This explains the interference pattern that we and another research group have detected.[12,13] It also explains why it is possible to detect the degree of polarization of a flat-lying wire. The absence of a directional lasing beam in the case of a sub-wavelength nanowire laser is an essential difference with macroscopic lasers. Li *et al.* calculated the lowest-energy modes in a ZnO nanowire assuming that the dielectric function is determined by exciton–photon coupling (see Fig. 4) and solving the Maxwell equations with a finite-element solver.[11] It was found that the two lowest energy modes are strongly linearly polarized and can be approximated with $E \perp$ long axis ($= c$-axis), and $k \parallel c$. The modes of lowest energy are best described as linearly polarized modes, although they are slightly more complex. Furthermore, the electric field spills over the ZnO nanowire cavity. Noteworthy, Li *et al.* also described that thicker nanowires (diameter of 600 nm) can show opposite lasing polarization, *i.e.* E $\parallel$ C polarization, pointing to a whispering gallery-like lasing mode, the existence of such a mode in a 600 nm wire was confirmed by the mode calculations. We note that non-lasing whispering gallery modes in ZnO nanowires with hexagonal symmetry have been reported both in the visible part of the spectrum (defect recombination) and in the polariton-regime.[60,64,173]

10. The lasing mechanism: exciton–polariton scattering, electron–hole recombination or more exotic?

In order to start the discussion on the mechanism of lasing, we first show results that we have obtained with a single wire lying on the substrate. Fig. 9 shows the onset and growth of a number of lasing modes out of the Fabry–Pérot luminescence modes.

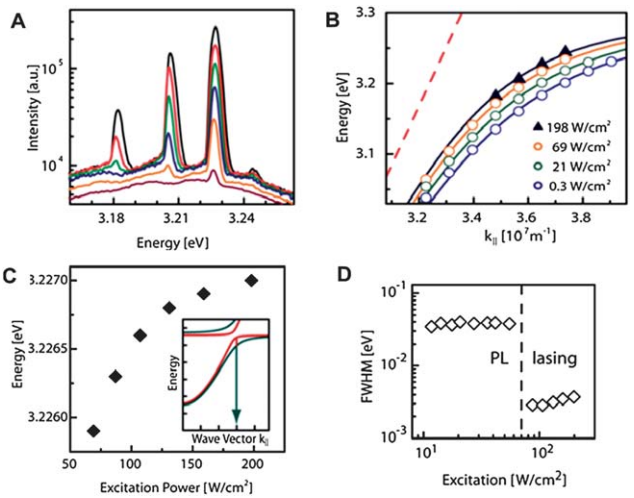

Fig. 9 Lasing characteristics of a single hexagonal ZnO nanowire (about 200 nm in diameter, 4 μm in length) lying on a silica substrate. (A) Lasing spectrum with increasing excitation power, (B) plot of the Fabry–Pérot modes in the energy–wave vector diagram, (C) position of the highest energy peak as a function of the excitation power, (D) full-width-half-maximum of a luminescence peak that evolves abruptly in a lasing peak.

Fig. 9D shows that the onset of lasing is characterised by an abrupt narrowing of the emission from about 40 meV (thermally broadened exciton) to about 2 meV. The energy *vs.* wave-vector relations of the Fabry–Pérot modes are presented in Fig. 9B, for increasing excitation intensity. In fact, the shape of the energy–wave vector plots of the lasing modes remains preserved and strongly curved; they can be fitted with the polariton eqn (5a) in a similar way as the luminescence modes. With increasing excitation intensity, each mode broadens and shifts gradually to higher energy. Time-resolved spectroscopy performed by Fallert *et al.*[63] at cryogenic temperatures with an upright nanowire showed the growth of new laser modes of lower quantum number m_z, and a blueshift of individual laser peaks with increasing excitation intensity, in a very similar way as reported above for a wire lying on the substrate.

At first sight, these data provide strong evidence that lasing is mediated by exciton–polaritons. In the exciton–polariton view, the blueshift of the lasing modes with the excitation intensity is explained by a weakening of the exciton binding energy by free carrier screening. The growth of new lasing modes at lower quantum numbers m_z with increasing excitation intensity reflects the increasing occupation of these modes by scattering processes. It should be noted that this cooling process does not lead to occupation of the $k_z = 0$ mode due to the large energy difference between the $k_z = 0$ minimum and the occupied modes. This forms a marked contrast to semiconductor quantum well lasers where the $k = 0$ condensation point could be reached by spontaneous cooling, leading to a Bose–Einstein condensate.[120,219,220]

Exciton–exciton (polariton–polariton) scattering has been put forward as the lasing mechanism in early and more recent works. On the basis of the very large longitudinal–transverse splitting, and hence huge oscillator strength of the exciton, Zamfirescu *et al.* stated that ZnO must be one of the best materials to achieve polariton lasing.[20] They calculated a (particle density–temperature) phase diagram for ZnO, showing considerable areas of polariton spontaneous emission and polariton lasing. This picture is contested by several other groups. Klingshirn *et al.*[30] stated that the thermal broadening of the exciton resonance (*i.e.* damping) at room-temperature is comparable to the exciton binding energy. Moreover the electron–hole attraction energy becomes screened by the other carriers; above the critical Mott density (about 0.5×10^{18} cm^{-3})[30] excitons are completely dissociated and an electron–hole plasma is formed. Klingshirn stated that although the densities in ZnO nanowires at the lasing threshold may reach the Mott-density, they are possibly still lower than the density required to shift the quasi-Fermi level of electrons and holes into the conduction and valence band respectively,[30] in order to reach the state of population inversion required for electron–hole lasing. In that respect it is important to note that the band gap decreases with increasing lattice temperature, but also with increasing density of electron and hole excitations. A gain model based on electron–hole band-to-band recombination in an electron–hole plasma has also been suggested to explain the results presented above.[63] The gain was calculated as a function of the photon energy, for increasing excitation densities. It was observed that a gain peak arises at a particle density of 10^{18} cm^{-3}, and extends to lower energy with increasing density, due to the band gap renormalization.

Versteegh *et al.*[132] developed a comprehensive many-body theory for optically excited ZnO taking into account a screened electron–hole interaction, Coulomb-repulsions and band gap renormalization. The theory provides strongly curved energy–wave vector diagrams nearly identical to the phenomenological polariton dispersion relation given by eqn (5a). The theory predicts the onset of gain at excitation densities that pertain to the electron–hole plasma regime. Hence, this very recent many-body theory assigns lasing strictly to the electron–hole plasma regime.

From the above it should be clear that the discussion on the lasing mechanism in ZnO has sharpened the pen and opinion of several research groups. We should keep in mind that lasing in ZnO has been observed in a wide temperature range, from cryogenic to (above) room temperature. Possibly, the mechanism responsible for gain may depend on the quality of the wires and the temperature. The authors of this review are convinced that more dedicated spectroscopy with non-resonant and resonant excitation using one, two or three photons on ZnO crystals with different geometries (macroscopic, quantum wells, wires, rods and dots) will resolve this issue eventually. On the other hand, we predict that interesting new "particle" physics involving polaritons or correlated electron–hole pairs will soon emerge in the semiconductor ZnO, and further enrich solid-state science.

11. Perspectives for ZnO opto-electronics

ZnO is an interesting semiconductor for application in opto-electronic devices, such as light-emitting diodes (LEDs), electrically pumped lasers, electron collection in photovoltaic cells, and as transparent conducting oxide.[221,259] This is partly based on the possibility to produce materials of sufficient quality and thus luminescence yield by various liquid-phase and gas-phase methods. Furthermore, the growth methods allow one to prepare not only bulk ZnO, but also polycrystalline thin-film systems, quantum wells, quantum dots, and rods and wires.[222] The

different geometries all have their specific applications.[223–225] The green defect and near UV band-gap luminescence can be used to excite phosphors for large scale white-light LEDs whereas arrays of ZnO wires may form the electron collector base for novel types of solar cells. The wire-like geometry forms the basis of a so-called "bulk-heterojunction" important for efficient carrier collection.

Regarding the electrically driven light-emitting devices and lasers, the problem of the lack of p-type ZnO has been circumvented in the past by n-type ZnO/p-type heterojunctions. The p-type material consists generally of GaN,[226–234] but organic hole conductors[231,235,236] and p-Si[237] have also been reported for efficient light emitting diodes. Since 2000, the first report on p-type ZnO emerged, and light emission from p/n and p/i/n ZnO homojunctions[76,238–244] and p-type ZnO/n-type Y (Y = Si or GaN)[245] have been reported. Electrically driven amplified spontaneous emission or lasing in the near UV at room temperature has been demonstrated with n-type ZnO coupled to p-GaN[246,247] but also with p-type ZnO coupled to n-Si.[250,251] Electrically driven single ZnO nanowire laser diodes still remain elusive but importantly electrically driven stimulated emission from ZnO nanowire layers has been obtained by either using n-type ZnO nanowires on p-Si[248] or p-type ZnO nanowires on n-Si.[249] Although p-type conductivity in ZnO is still under intense debate and is not yet technologically mature,[258] these first reports make us believe that arrays of ZnO nanowires and single ZnO nanowires will play a key role in electrically pumped near-UV lasers of the future allowing for instance higher data densities in optical storage solutions, nanophotonic computation and (bio) medical diagnostics.

Notes and references

1 A. Einstein, *Phys. Z.*, 1917, **18**, 121.
2 B. Bransden and H. Joachain, *Quantum Mechanics*, C.J. Pearson Education Limited, 2000, ISBN: 0582-35691-1.
3 T. H. Maiman, *Nature*, 1960, **187**, 493.
4 T. H. Maiman, *J. Opt. Soc. Am.*, 1960, **50**, 1134.
5 T. H. Maiman, *Phys. Rev.*, 1961, **123**, 1145.
6 T. H. Maiman, V. Evtuhov, R. H. Hoskins, I. J. Dhaenens and C. K. Asawa, *Phys. Rev.*, 1961, **123**, 1151.
7 R. N. Hall, R. O. Carlson, T. J. Soltys, G. E. Fenner and J. D. Kingsley, *Phys. Rev. Lett.*, 1962, **9**, 366.
8 R. N. Hall, *Solid-State Electron.*, 1963, **6**, 405.
9 F. H. Nicoll, *Appl. Phys. Lett.*, 1966, **9**, 13.
10 M. H. Huang, S. Mao, H. Feick, H. Yan, Y. Wu, H. Kind, E. Weber, R. Russo and P. Yang, *Science*, 2001, **292**, 1897.
11 H. Y. Li, S. Ruhle, R. Khedoe, A. F. Koenderink and D. Vanmaekelbergh, *Nano Lett.*, 2009, **9**, 3515.
12 J. C. Johnson, H. Q. Yan, P. D. Yang and R. J. Saykally, *J. Phys. Chem. B*, 2003, **107**, 8816.
13 L. K. Van Vugt, S. Ruhle and D. Vanmaekelbergh, *Nano Lett.*, 2006, **6**, 2707.
14 J. M. Hvam, *Solid State Commun.*, 1973, **12**, 95.
15 D. C. Reynolds, D. C. Look and B. Jogai, *Solid State Commun.*, 1996, **99**, 873.
16 D. M. Bagnall, Y. F. Chen, Z. Zhu, T. Yao, S. Koyama, M. Y. Shen and T. Goto, *Appl. Phys. Lett.*, 1997, **70**, 2230.
17 P. Yu, Z. K. Tang, G. K. L. Wong, M. Kawasaki, A. Ohtomo, H. Koinuma and Y. Segawa, *J. Cryst. Growth*, 1998, **184**, 601.
18 Z. K. Tang, G. K. L. Wong, P. Yu, M. Kawasaki, A. Ohtomo, H. Koinuma and Y. Segawa, *Appl. Phys. Lett.*, 1998, **72**, 3270.
19 S. L. Cho, J. Ma, Y. K. Kim, Y. Sun, G. K. L. Wong and J. B. Ketterson, *Appl. Phys. Lett.*, 1999, **75**, 2761.
20 M. Zamfirescu, A. Kavokin, B. Gil, G. Malpuech and M. Kaliteevski, *Phys. Rev. B: Condens. Matter*, 2002, **65**, 161205.
21 K. Govender, D. S. Boyle, P. O'Brien, D. Binks, D. West and D. Coleman, *Adv. Mater.*, 2002, **14**, 1221.
22 H. Q. Yan, J. Johnson, M. Law, R. R. He, K. Knutsen, J. R. McKinney, J. Pham, R. Saykally and P. D. Yang, *Adv. Mater.*, 2003, **15**, 1907.
23 J. C. Johnson, H. Yan, P. Yang and R. J. Saykally, *J. Phys. Chem. B*, 2003, **107**, 8816.
24 H. Q. Yan, R. R. He, J. Johnson, M. Law, R. J. Saykally and P. D. Yang, *J. Am. Chem. Soc.*, 2003, **125**, 4728.
25 J. C. Johnson, K. P. Knutsen, H. Q. Yan, M. Law, Y. F. Zhang, P. D. Yang and R. J. Saykally, *Nano Lett.*, 2004, **4**, 197.
26 S. F. Yu, C. Yuen, S. P. Lau, W. I. Park and G. C. Yi, *Appl. Phys. Lett.*, 2004, **84**, 3241.
27 T. Nobis, E. M. Kaidashev, A. Rahm, M. Lorenz and M. Grundmann, *Phys. Rev. Lett.*, 2004, **93**, 103903.
28 M. Law, D. J. Sirbuly, J. C. Johnson, J. Goldberger, R. J. Saykally and P. Yang, *Science*, 2004, **305**, 1269.
29 C. Klingshirn, J. Fallert, H. Zhou and H. Kalt, *Appl. Phys. Lett.*, 2007, **91**, 126101.
30 C. Klingshirn, R. Hauschild, J. Fallert and H. Kalt, *Phys. Rev. B: Condens. Matter Mater. Phys.*, 2007, **75**, 115203.
31 J. Fallert, R. J. B. Dietz, M. Hauser, F. Stelzl, C. Klingshirn and H. Kalt, *J. Lumin.*, 2009, **129**, 1685.
32 D. J. Gargas, M. E. Toimil-Molares and P. D. Yang, *J. Am. Chem. Soc.*, 2009, **131**, 2125.
33 X. Duan, Y. Huang, R. Agarwal and C. M. Lieber, *Nature*, 2003, **421**, 241.
34 L. K. van Vugt, S. J. Veen, E. Bakkers, A. L. Roest and D. Vanmaekelbergh, *J. Am. Chem. Soc.*, 2005, **127**, 12357.
35 M. H. M. v. Weert, O. Wunnicke, A. L. Roest, T. J. Eijkemans, A. Y. Silov, J. E. M. Haverkort, G. W. t. Hooft and E. P. A. M. Bakkers, *Appl. Phys. Lett.*, 2006, **88**, 043109.
36 E. P. A. M. Bakkers, J. A. v. Dam, S. D. Franceschi, L. P. Kouwenhoven, M. Kaiser, M. Verheijen, H. Wondergem and P. V. D. Sluis, *Nat. Mater.*, 2004, **3**, 769.
37 R. E. Algra, M. A. Verheijen, M. T. Borgstrom, L. F. Feiner, G. Immink, W. J. P. van Enckevort, E. Vlieg and E. Bakkers, *Nature*, 2008, **456**, 369.
38 B. Hua, J. Motohisa, Y. Kobayashi, S. Hara and T. Fukui, *Nano Lett.*, 2009, **9**, 112.
39 A. V. Maslov and C. Z. Ning, *Appl. Phys. Lett.*, 2003, **83**, 1237.
40 A. V. Maslov and C. Z. Ning, *IEEE J. Quantum Electron.*, 2004, **40**, 1389.
41 A. V. Maslov and C. Z. Ning, *Opt. Lett.*, 2004, **29**, 572.
42 Z. Y. Li and K. M. Ho, *Phys. Rev. B: Condens. Matter Mater. Phys.*, 2005, **71**, 045315.
43 L. K. van Vugt, B. Piccione and R. Agarwal, *Appl. Phys. Lett.*, 2010, **97**, 061115.
44 L. K. van Vugt, B. Zhang, B. Piccione, A. A. Spector and R. Agarwal, *Nano Lett.*, 2009, **9**, 1684.
45 S. Y. Hu, M. S. Miller, D. B. Young, J. C. Yi, D. Leonard, A. C. Gossard, P. M. Petroff, L. A. Coldren and N. Dagli, *Appl. Phys. Lett.*, 1993, **63**, 2015.
46 J. C. Johnson, H. Q. Yan, R. D. Schaller, L. H. Haber, R. J. Saykally and P. D. Yang, *J. Phys. Chem. B*, 2001, **105**, 11387.
47 J. C. Johnson, H. J. Choi, K. P. Knutsen, R. D. Schaller, P. D. Yang and R. J. Saykally, *Nat. Mater.*, 2002, **1**, 106.
48 R. Agarwal, C. J. Barrelet and C. M. Lieber, *Nano Lett.*, 2005, **5**, 917.
49 J. K. Song, J. M. Szarko, S. R. Leone, S. H. Li and Y. P. Zhao, *J. Phys. Chem. B*, 2005, **109**, 15749.
50 A. B. Greytak, C. J. Barrelet, Y. Li and C. M. Lieber, *Appl. Phys. Lett.*, 2005, **87**, 151103.
51 S. Gradecak, F. Qian, Y. Li, H. G. Park and C. M. Lieber, *Appl. Phys. Lett.*, 2005, **87**, 173111.
52 S. Hirano, N. Takeuchi, S. Shimada, K. Masuya, K. Ibe, H. Tsunakawa and M. Kuwabara, *J. Appl. Phys.*, 2005, **98**.
53 T. Nobis and M. Grundmann, *Phys. Rev. A: At., Mol., Opt. Phys.*, 2005, **72**.
54 P. J. Pauzauskie, D. J. Sirbuly and P. D. Yang, *Phys. Rev. Lett.*, 2006, **96**, 143903.
55 L. Chen and E. Towe, *Appl. Phys. Lett.*, 2006, **89**, 053125.

56 C. F. Zhang, Z. W. Dong, G. J. You, S. X. Qian and H. Deng, *Opt. Lett.*, 2006, **31**, 3345.
57 L. K. van Vugt, S. Rühle and D. Vanmaekelbergh, *Ned. Tijdschr. Natuurkd.*, 2006, **72**, 398.
58 B. L. Cao, Y. Jiang, C. Wang, W. H. Wang, L. Z. Wang, M. Niu, W. J. Zhang, Y. Q. Li and S. T. Lee, *Adv. Funct. Mater.*, 2007, **17**, 1501.
59 H. G. Park, F. Qian, C. J. Barrelet and Y. Li, *Appl. Phys. Lett.*, 2007, **91**, 251115.
60 L. X. Sun, Z. H. Chen, Q. J. Ren, K. Yu, L. H. Bai, W. H. Zhou, H. Xiong, Z. Q. Zhu and X. C. Shen, *Phys. Rev. Lett.*, 2008, **100**, 156403.
61 J. K. Song, U. Willer, J. M. Szarko, S. R. Leone, S. Li and Y. Zhao, *J. Phys. Chem. C*, 2008, **112**, 1679.
62 Y. S. Zhao, A. D. Peng, H. B. Fu, Y. Ma and J. N. Yao, *Adv. Mater.*, 2008, **20**, 1661.
63 J. Fallert, F. Stelzl, H. Zhou, A. Reiser, K. Thonke, R. Sauer, C. Klingshirn and H. Kalt, *Opt. Express*, 2008, **16**, 1125.
64 C. Czekalla, C. Sturm, R. Schmidt-Grund, B. Q. Cao, M. Lorenz and M. Grundmann, *Appl. Phys. Lett.*, 2008, **92**, 241102.
65 T. Voss, G. T. Svacha, E. Mazur, S. Muller and C. Ronning, *Nanotechnology*, 2009, **20**, 095702.
66 C. F. Zhang, F. Zhang, T. Xia, N. Kumar, J. I. Hahm, J. Liu, Z. L. Wang and J. Xu, *Opt. Express*, 2009, **17**, 7893.
67 V. V. Ursaki, V. V. Zalamai, I. M. Tiginyanu, A. Burlacu, E. V. Rusu and C. Klingshirn, *Appl. Phys. Lett.*, 2009, **95**, 171101.
68 V. V. Zalamai, V. V. Ursaki, C. Klingshirn, H. Kalt, G. A. Emelchenko and A. N. Redkin, *Appl. Phys. B: Lasers Opt.*, 2009, **97**, 817.
69 M. A. Zimmler, F. Capasso, S. Muller and C. Ronning, *Semicond. Sci. Technol.*, 2010, **25**, 024001.
70 Ü. Özgür, Y. I. Alivov, C. Liu, A. Teke, M. A. Reshchikov, S. Doğan, V. Avrutin, S. J. Cho and H. Morkoç, *J. Appl. Phys.*, 2005, **98**, 041301.
71 M. Joseph, H. Tabata and T. Kawai, *Jpn. J. Appl. Phys.*, 1999, **38**, L1205.
72 T. Yamamoto and H. Katayama-Yoshida, *Jpn. J. Appl. Phys.*, 1999, **38**, L166.
73 Y. R. Ryu, S. Zhu, D. C. Look, J. M. Wrobel, H. M. Jeong and H. W. White, *J. Cryst. Growth*, 2000, **216**, 330.
74 M. Joseph, H. Tabata, H. Saeki, K. Ueda and T. Kawai, *Phys. B (Amsterdam, Neth.)*, 2001, **302**, 140.
75 S. B. Zhang, S. H. Wei and A. Zunger, *Phys. Rev. B: Condens. Matter*, 2001, **63**, 075205.
76 A. Tsukazaki, A. Ohtomo, T. Onuma, M. Ohtani, T. Makino, M. Sumiya, K. Ohtani, S. F. Chichibu, S. Fuke, Y. Segawa, H. Ohno, H. Koinuma and M. Kawasaki, *Nat. Mater.*, 2005, **4**, 42.
77 D. C. Look, D. C. Reynolds, C. W. Litton, R. L. Jones, D. B. Eason and G. Cantwell, *Appl. Phys. Lett.*, 2002, **81**, 1830.
78 K. K. Kim, H. S. Kim, D. K. Hwang, J. H. Lim and S. J. Park, *Appl. Phys. Lett.*, 2003, **83**, 63.
79 E. C. Lee and K. J. Chang, *Phys. Rev. B: Condens. Matter Mater. Phys.*, 2004, **70**, 115210.
80 M. G. Wardle, J. P. Goss and P. R. Briddon, *Phys. Rev. B: Condens. Matter Mater. Phys.*, 2005, **71**, 115205.
81 M. Kawasaki, A. Ohtomo, H. Koinuma, Y. Sakurai, Y. Yoshida, Z. K. Tang, P. Yu, G. K. L. Wang and Y. Segawa, in *Silicon Carbide, III-Nitrides and Related Materials, Pts 1 and 2*, ed. G. Pensl, H. Morkoc, B. Monemar and E. Janzen, 1998, vol. 264-2, p. 1459.
82 J. F. Muth, R. M. Kolbas, A. K. Sharma, S. Oktyabrsky and J. Narayan, *J. Appl. Phys.*, 1999, **85**, 7884.
83 B. Gil, *Phys. Rev. B: Condens. Matter*, 2001, **64**, 201310.
84 S. F. Chichibu, T. Sota, G. Cantwell, D. B. Eason and C. W. Litton, *J. Appl. Phys.*, 2003, **93**, 756.
85 E. McGlynn, J. Fryar, M. O. Henry, J.-P. Mosnier, J. G. Lunney, D. O. Mahony and E. dePosada, *Phys. B (Amsterdam, Neth.)*, 2003, **340–342**, 230.
86 X. Q. Zhang, Z. K. Tang, M. Kawasaki, A. Ohtomo and H. Koinuma, *J. Phys.: Condens. Matter*, 2003, **15**, 5191.
87 A. A. Toropov, O. V. Nekrutkina, T. V. Shubina, T. Gruber, C. Kirchner, A. Waag, K. F. Karlsson, P. O. Holtz and B. Monemar, *Phys. Rev. B: Condens. Matter Mater. Phys.*, 2004, **69**, 165205.
88 Y. R. Ryu, J. A. Lubguban, T. S. Lee, H. W. White, T. S. Jeong, C. J. Youn and B. J. Kim, *Appl. Phys. Lett.*, 2007, **90**, 131115.
89 A. B. Djurisic and Y. H. Leung, *Small*, 2006, **2**, 944.
90 S. Mahamuni, K. Borgohain, B. S. Bendre, V. J. Leppert and S. H. Risbud, *J. Appl. Phys.*, 1999, **85**, 2861.
91 A. v. Dijken, E. A. Meulenkamp, D. Vanmaekelbergh and A. Meijerink, *J. Lumin.*, 2000, **90**, 123.
92 A. L. Roest, J. J. Kelly, D. Vanmaekelbergh and E. A. Meulenkamp, *Phys. Rev. Lett.*, 2002, **89**, 036801.
93 H. Zhou, H. Alves, D. M. Hofmann, W. Kriegseis, B. K. Meyer, G. Kaczmarczyk and A. Hoffmann, *Appl. Phys. Lett.*, 2002, **80**, 210.
94 H. Zhou, H. Alves, D. M. Hofmann, B. K. Meyer, G. Kaczmarczyk, A. Hoffmann and C. Thomsen, *Phys. Status Solidi B*, 2002, **229**, 825.
95 A. L. Roest, A. Germeau, J. J. Kelly, D. Vanmaekelbergh, G. Allan and E. A. Meulenkamp, *ChemPhysChem*, 2003, **4**, 959.
96 Y. H. Lin, D. J. Wang, Q. D. Zhao, M. Yang and Q. L. Zhang, *J. Phys. Chem. B*, 2004, **108**, 3202.
97 C. W. Cheng, B. Liu, E. J. Sie, W. W. Zhou, J. X. Zhang, H. Gong, C. H. A. Huan, T. C. Sum, H. D. Sun and H. J. Fan, *J. Phys. Chem. C*, 2010, **114**, 3863.
98 A. van Dijken, E. A. Meulenkamp, D. Vanmaekelbergh and A. Meijerink, *J. Lumin.*, 2000, **87–89**, 454.
99 A. van Dijken, E. A. Meulenkamp, D. Vanmaekelbergh and A. Meijerink, *J. Phys. Chem. B*, 2000, **104**, 4355.
100 A. Van Dijken, E. A. Meulenkamp, D. Vanmaekelbergh and A. Meijerink, *J. Phys. Chem. B*, 2000, **104**, 1715.
101 A. V. Rodina, M. Strassburg, M. Dworzak, U. Haboek, A. Hoffman, A. Zeuner, H. R. Alves, D. M. Hofmann and B. K. Meyer, *Phys. Rev. B: Condens. Matter Mater. Phys.*, 2004, **69**, 125206.
102 A. Teke, Ü. Özgür, S. Doğan, X. Gu, H. Morkoç, B. Nemeth, J. Nause and H. O. Everitt, *Phys. Rev. B: Condens. Matter Mater. Phys.*, 2004, **70**, 195207.
103 W. R. L. Lambrecht, A. V. Rodina, S. Limpijumnong, B. Segall and B. K. Meyer, *Phys. Rev. B: Condens. Matter*, 2002, **65**, 075207.
104 C. Klingshirn, J. Fallert, H. Zhou, J. Sartor, C. Thiele, F. Maier-Flaig, D. Schneider and H. Kalt, *Phys. Status Solidi B*, 2010, **247**, 1424.
105 C. Klingshirn, J. Fallert, R. Hauschild, M. Hauser, H. Kalt and H. J. Zhou, *J. Korean Phys. Soc.*, 2008, **53**, 2800.
106 J. J. Hopfield, *Phys. Rev.*, 1958, **112**, 1555.
107 J. J. Hopfield and D. G. Thomas, *J. Phys. Chem. Solids*, 1960, **12**, 276.
108 J. J. Hopfield and D. G. Thomas, *Phys. Rev. Lett.*, 1965, **15**, 22.
109 C. B. a. l. Guillaume, A. Bonnot and J. M. Debever, *Phys. Rev. Lett.*, 1970, **24**, 1235.
110 V. A. Kiselev, B. S. Razbirin and I. N. Uraltsev, *Phys. Status Solidi B*, 1975, **72**, 161.
111 I. V. Makarenko, I. N. Uraltsev and V. A. Kiselev, *Phys. Status Solidi B*, 1980, **98**, 773.
112 J. Lagois, *Phys. Rev. B*, 1981, **23**, 5511.
113 R. Houdré, R. P. Stanley, U. Oesterle, M. Ilegems and C. Weisbuch, *Phys. Rev. B: Condens. Matter*, 1994, **49**, 16761.
114 C. Boemare, *Phys. Rev. B: Condens. Matter*, 1995, **51**, 7954.
115 V. Savona, F. Tassone, C. Piermarocchi and A. Quattropani, *Phys. Rev. B: Condens. Matter*, 1996, **53**, 13051.
116 F. Tassone, C. Piermarocchi, V. Savona, A. Quattropani and P. Schwendimann, *Phys. Rev. B: Condens. Matter*, 1997, **56**, 7554.
117 D. Snoke, *Science*, 2002, **298**, 1368.
118 H. Deng, G. Weihs, D. Snoke, J. Bloch and Y. Yamamoto, *Proc. Natl. Acad. Sci. U. S. A.*, 2003, **100**, 15318.
119 M. J. Hartmann, F. Brandao and M. B. Plenio, *Nat. Phys.*, 2006, **2**, 849.
120 J. Kasprzak, M. Richard, S. Kundermann, A. Baas, P. Jeambrun, J. M. J. Keeling, F. M. Marchetti, M. H. Szymanska, R. Andre, J. L. Staehli, V. Savona, P. B. Littlewood, B. Deveaud and L. S. Dang, *Nature*, 2006, **443**, 409.
121 L. K. van Vugt, S. Ruhle, P. Ravindran, H. C. Gerritsen, L. Kuipers and D. Vanmaekelbergh, *Phys. Rev. Lett.*, 2006, **97**, 4.
122 Y. Fu, L. Thylen and H. Agren, *Nano Lett.*, 2008, **8**, 1551.
123 R. Schmidt-Grund, B. Rheinlander, C. Czekalla, G. Benndorf, H. Hochmuth, M. Lorenz and M. Grundmann, *Appl. Phys. B: Lasers Opt.*, 2008, **93**, 331.
124 X. Zhang, P. Wang, X. Zhang, J. Xu, Y. Zhu and D. Yu, *Nano Res.*, 2009, **2**, 47.

125 C. Weisbuch, M. Nishioka, A. Ishikawa and Y. Arakawa, *Phys. Rev. Lett.*, 1992, **69**, 3314.
126 A. I. Tartakovskii, V. D. Kulakovski, Y. I. Koval, T. B. Borzenko, A. Forchel and J. P. Reithmaier, *J. Exp. Theor. Phys.*, 1998, **87**, 723.
127 C. Weisbuch, H. Benisty and R. Houdre, *J. Lumin.*, 2000, **85**, 271.
128 J. P. Reithmaier, *Semicond. Sci. Technol.*, 2008, **23**, 123001.
129 Y. Chen, A. Tredicucci and F. Bassani, *Phys. Rev. B: Condens. Matter*, 1995, **52**, 1800.
130 J. Lagois, *Phys. Rev. B: Solid State*, 1977, **16**, 1699.
131 B. Gil and A. V. Kavokin, *Appl. Phys. Lett.*, 2002, **81**, 748.
132 M. Versteegh, T. Kuis, H. T. C. Stoof and J. I. Dijkhuis, *Phys. Rev. B: Condens. Matter Mater. Phys.*, arXiv:1012.3600v2.
133 S. Ruhle, L. K. van Vugt, H. Y. Li, N. A. Keizer, L. Kuipers and D. Vanmaekelbergh, *Nano Lett.*, 2008, **8**, 119.
134 L. E. Li and L. N. Demyanets, *Crystallogr. Rep.*, 2008, **53**, 671.
135 T. Pauporté, D. Lincot, B. Viana and F. Pellé, *Appl. Phys. Lett.*, 2006, **89**, 233112.
136 J.-H. Choy, E.-S. Jang, J.-H. Won, J.-H. Chung, D.-J. Jang and Y.-W. Kim, *Adv. Mater.*, 2003, **15**, 1911.
137 Z. Qiu, K. S. Wong, M. Wu, W. Lin and H. Xu, *Appl. Phys. Lett.*, 2004, **84**, 2739.
138 W. I. Park, D. H. Kim, S.-W. Jung and G.-C. Yi, *Appl. Phys. Lett.*, 2002, **80**, 4232.
139 Y. Zhang, S. S. Mao and R. E. Russo, *Appl. Phys. Lett.*, 2005, **87**, 043106.
140 R. Q. Guo, J. Nishimura, M. Matsumoto, M. Higashihata, D. Nakamura, J. Suehiro and T. Okada, *Appl. Phys. B: Lasers Opt.*, 2008, **90**, 539.
141 D. Yu, L. Hu, J. Li, H. Hu, H. Zhang, Z. Zhao and Q. Fu, *Mater. Lett.*, 2008, **62**, 4063.
142 J. K. Song, J. M. Szarko, S. R. Leone, S. Li and Y. Zhao, *J. Phys. Chem. B*, 2005, **109**, 15749.
143 V. V. Ursaki, V. V. Zalamai, A. Burlacu, J. Fallert, C. Klingshirn, H. Kalt, G. A. Emelchenkoc, A. N. Redkin, A. N. Gruzintsev, E. V. Rusue and I. M. Tiginyanu, *Superlattices Microstruct.*, 2009, **46**, 513.
144 A. N. Gruzintsev, G. A. Emelchenko, A. N. Red'kin, W. T. Volkov, E. E. Yakimov and G. Visimberga, *Semiconductors*, 2010, **44**, 1217.
145 M. H. Huang, Y. Wu, H. Feick, N. Tran, E. Weber and P. Yang, *Adv. Mater.*, 2001, **13**, 113.
146 The catalytic nanoparticles are often found on the substrate surface, between the wires of the array.
147 C. F. Zhang, Z. W. Dong, G. J. You, R. Y. Zhu, S. X. Qiana, H. Deng, H. Cheng and J. C. Wang, *Appl. Phys. Lett.*, 2006, **89**, 042117.
148 H. Zhou, M. Wissinger, J. Fallert, R. Hauschild, F. Stelzl, C. Klingshirn and H. Kalt, *Appl. Phys. Lett.*, 2007, **91**, 181112.
149 M. A. Zimmler, J. Bao, F. Capasso, S. Müller and C. Ronning, *Appl. Phys. Lett.*, 2008, **93**, 051101.
150 L. Cao, B. Zou, C. Li, Z. Zhang, S. Xie and G. Yang, *Europhys. Lett.*, 2004, **68**, 740.
151 J. Dai, C. X. Xu, P. Wu, J. Y. Guo, Z. H. Li and Z. L. Shi, *Appl. Phys. Lett.*, 2010, **97**, 011101.
152 B. Zou, R. Liu, F. Wang, A. Pan, L. Cao and Z. L. Wang, *J. Phys. Chem. B*, 2006, **110**, 12865.
153 Y. G. Wang, C. Yuen, S. P. Lau, S. F. Yu and B. K. Tay, *Chem. Phys. Lett.*, 2003, **377**, 329.
154 K. Bando, T. Sawabe, K. Asaka and Y. Masumoto, *J. Lumin.*, 2004, **108**, 385.
155 X. Han, G. Wang, Q. Wang, L. Cao, R. Liu, B. Zou and J. G. Hou, *Appl. Phys. Lett.*, 2005, **86**, 223106.
156 M. Zacharias, K. Subannajui, A. Menzel and Y. Yang, *Phys. Status Solidi B*, 2010, **247**, 2305.
157 P. Fons, K. Iwata, A. Yamada, K. Matsubara, S. Niki, K. Nakahara, T. Tanabe and H. Takasu, *Appl. Phys. Lett.*, 2004, **77**, 1801.
158 H. J. Fan, F. Fleischer, W. Lee, K. Nielsch, R. Scholz, M. Zacharias, U. Gosele, A. Dadgar and A. Krost, *Superlattices Microstruct.*, 2004, **36**, 95.
159 T. W. K. S. Yoon, *J. Cryst. Growth*, 2000, **212**, 411.
160 G. M. Prinz, A. Reiser, T. Röder, M. Schirra, M. Feneberg, U. R. Sauer and K. Thonke, *Appl. Phys. Lett.*, 2007, **90**, 233115.
161 R. S. Wagner and W. C. Ellis, *Appl. Phys. Lett.*, 1964, **4**, 89.
162 C. Borchers, S. Muller, D. Stichtenoth, D. Schwen and C. Ronning, *J. Phys. Chem. B*, 2006, **110**, 1656.
163 J. B. Baxter, F. Wu and E. S. Aydil, *Appl. Phys. Lett.*, 2003, **83**, 3797.
164 W.-J. Li, E.-W. Shi, W.-Z. Zhong and Z.-W. Yin, *J. Cryst. Growth*, 1999, **203**, 186.
165 Y. Wu and P. Yang, *J. Am. Chem. Soc.*, 2001, **123**, 3165.
166 M. S. Gudiksen, J. Wang and C. M. Lieber, *J. Phys. Chem. B*, 2001, **105**, 4062.
167 A. N. Gruzintsev, G. A. Emelchenko, A. N. Redkin, W. T. Volkov, E. E. Yakimov and G. Visimberga, *Semiconductors*, 2010, **44**, 1235.
168 V. V. Zalamai, V. V. Ursaki, C. Klingshirn, H. Kalt, G. A. Emelchenko and A. N. Redkin, *Appl. Phys. B: Lasers Opt.*, 2009, **97**, 817.
169 M. H. Huang, S. Mao, H. Feick, H. Yan, Y. Wu, H. Kind, E. Weber, R. Russo and P. Yang, *Science*, 2001, **292**, 1897.
170 J. Hu, L.-s. Li, W. Yang, L. Manna, L.-w. Wang and A. P. Alivisatos, *Science*, 2001, **292**, 2060.
171 P. J. Pauzauskie, D. Talaga, K. Seo, P. Yang and F. Lagugne-Labarthet, *J. Am. Chem. Soc.*, 2005, **127**, 17146.
172 J. Wang, M. S. Gudiksen, X. Duan, Y. Cui and C. M. Lieber, *Science*, 2001, **293**, 1455.
173 D. Wang, H. W. Seo, C. C. Tin, M. J. Bozack, J. R. Williams, M. Park and Y. Tzeng, *J. Appl. Phys.*, 2006, **99**, 093112.
174 Y. Li, G. W. Meng, L. D. Zhang and F. Phillipp, *Appl. Phys. Lett.*, 2000, **76**, 2011.
175 M. Z. Wu, L. Z. Yao, W. L. Cai, G. W. Jiang, X. G. Li and Z. Yao, *Mater. Sci. Technol.*, 2004, **20**, 11.
176 W. Chen, X. M. Tao, Y. Y. Liu, X. H. Sun, Z. G. Hu and B. Fei, *Appl. Surf. Sci.*, 2006, **252**, 8683.
177 Y. R. Lin, S. S. Yang, S. Y. Tsai, H. C. Hsu, S. T. Wu and I. C. Chen, *Cryst. Growth Des.*, 2006, **6**, 1951.
178 Y. Xia, P. Yang, Y. Sun, Y. Wu, B. Mayers, B. Gates, Y. Yin, F. Kim and H. Yan, *Adv. Mater.*, 2003, **15**, 353.
179 Y. Sun, N. G. Ndifor-Angwafor, D. J. Riley and M. N. R. Ashfold, *Chem. Phys. Lett.*, 2006, **431**, 352.
180 F. Xu, Z. Y. Yuan, G. H. Du, T. Z. Ren, C. Bouvy, M. Halasa and B. L. Su, *Nanotechnology*, 2006, **17**, 588.
181 F. Xu, Z. Y. Yuan, G. H. Du, T. Z. Ren, C. Volcke, P. Thiry and B. L. Su, *J. Non-Cryst. Solids*, 2006, **352**, 2569.
182 D. S. Xue and Y. Gong, *Chin. Phys. Lett.*, 2006, **23**, 3105.
183 R. Guo, J. Nishimura, M. Matsumoto, M. Higashihata, D. Nakamura and T. Okada, *Appl. Phys. B: Lasers Opt.*, 2009, **94**, 33.
184 P. G. Li, W. H. Tang and X. Wang, *J. Alloys Compd.*, 2009, **479**, 634.
185 J. Y. Kim, H. W. Shim, E. K. Suh, T. Y. Kim, S. H. Lee, Y. J. Mo and K. S. Nahm, *J. Korean Phys. Soc.*, 2004, **44**, 137.
186 R. Prasanth, L. K. Van Vugt, D. A. M. Vanmaekelbergh and H. C. Gerritsen, *Appl. Phys. Lett.*, 2006, **88**, 181501.
187 L. Shi, Y. M. Xu, S. K. Hark, Y. Liu, S. Wang, L. M. Peng, K. W. Wong and Q. Li, *Nano Lett.*, 2007, **7**, 3559.
188 J. Zuniga-Perez, A. Rahm, C. Czekalla, J. Lenzner, M. Lorenz and M. Grundmann, *Nanotechnology*, 2007, **18**, 195303.
189 C. Czekalla, J. Guinard, C. Hanisch, B. Q. Cao, E. M. Kaidashev, N. Boukos, A. Travlos, J. Renard, B. Gayral, D. L. Dang, M. Lorenz and M. Grundmann, *Nanotechnology*, 2008, **19**, 115202.
190 R. Tena-Zaera, J. Elias and C. Levy-Clement, *Appl. Phys. Lett.*, 2008, **93**, 233119.
191 S. N. Bai and T. Y. Tseng, *J. Mater. Sci.: Mater. Electron.*, 2009, **20**, 604.
192 T. Ghoshal, S. Biswas, S. Kar and S. K. De, *J. Nanosci. Nanotechnol.*, 2009, **9**, 5586.
193 T. Ghoshal, S. Biswas, S. Kar, A. Dev, S. Chakrabarti and S. Chaudhuri, *Nanotechnology*, 2008, **19**, 065606.
194 M. Lorenz, J. Lenzner, E. M. Kaidashev, H. Hochmuth and M. Grundmann, *Ann. Phys.*, 2004, **13**, 39.
195 H. J. Fan, R. Scholz, M. Zacharias, U. Gosele, F. Bertram, D. Forster and J. Christen, *Appl. Phys. Lett.*, 2005, **86**, 023113.
196 X. B. He, T. Z. Yang, J. M. Cai, C. D. Zhang, H. M. Guo, D. X. Shi, C. M. Shen and H. J. Gao, *Chin. Phys. B*, 2008, **17**, 3444.
197 H. Z. Xue, N. Pan, R. G. Zeng, M. Li, X. Sun, Z. J. Ding, X. P. Wang and J. G. Hou, *J. Phys. Chem. C*, 2009, **113**, 12715.
198 M. J. Zhou, H. J. Zhu, Y. Jiao, Y. Y. Rao, S. Hark, Y. Liu, L. M. Peng and Q. Li, *J. Phys. Chem. C*, 2009, **113**, 8945.
199 S. Y. Zhang, R. Q. Liang, Q. R. Ou, X. J. Wu, M. F. Jiang, Z. F. Nie, F. Liu, X. J. Chang, Y. P. Wang, J. Du, P. J. Wang and Q. Q. Xin, *Electrochem. Solid-State Lett.*, 2009, **12**, H329.

200 C. Y. Chang, F. C. Tsao, C. J. Pan, G. C. Chi, H. T. Wang, J. J. Chen, F. Ren, D. P. Norton, S. J. Pearton, K. H. Chen and L. C. Chen, *Appl. Phys. Lett.*, 2006, **88**, 173503.
201 M. C. Jeong, B. Y. Oh, M. H. Ham, S. W. Lee and J. M. Myoung, *Small*, 2007, **3**, 568.
202 M. C. Jeong, B. Y. Oh, M. H. Ham and J. M. Myoung, *Appl. Phys. Lett.*, 2006, **88**, 202105.
203 Y. L. Chang, Q. F. Zhang, H. Sun and J. L. Wu, *Acta Phys. Sin.*, 2007, **56**, 2399.
204 Y. X. Wang, Q. F. Zhang, H. Sun, Y. L. Chang and J. L. Wu, *Acta Phys. Sin.*, 2008, **57**, 1141.
205 H. Sun, Q. Zhang, J. Zhang, T. Deng and J. Wu, *Appl. Phys. B: Lasers Opt.*, 2008, **90**, 543.
206 J. Y. Zhang, P. J. Li, H. Sun, X. Shen, T. S. Deng, K. T. Zhu, Q. F. Zhang and J. L. Wu, *Appl. Phys. Lett.*, 2008, **93**, 021116.
207 J. Q. Hu, Z. G. Chen, Y. G. Sun, H. Jiang, N. Wang and R. J. Zou, *J. Mater. Chem.*, 2009, **19**, 7011.
208 K. J. Chen, F. Y. Hung, S. J. Chang and S. J. Young, *J. Alloys Compd.*, 2009, **479**, 674.
209 J. Y. Wang, C. Y. Lee, Y. T. Chen, C. T. Chen, Y. L. Chen, C. F. Lin and Y. F. Chen, *Appl. Phys. Lett.*, 2009, **95**, 131117.
210 J. M. Bao, M. A. Zimmler, F. Capasso, X. W. Wang and Z. F. Ren, *Nano Lett.*, 2006, **6**, 1719.
211 M. A. Zimmler, T. Voss, C. Ronning and F. Capasso, *Appl. Phys. Lett.*, 2009, **94**, 241120.
212 Y. He, J. A. Wang, X. B. Chen, W. F. Zhang, X. Y. Zeng and Q. W. Gu, *J. Nanopart. Res.*, 2010, **12**, 169.
213 K. Kim, J. Kang, M. Lee, C. Yoon, K. Cho and S. Kim, *Jpn. J. Appl. Phys.*, 2010, **49**, 103538.
214 H. Z. Xue, N. Pan, M. Li, Y. K. Wu, X. P. Wang and J. G. Hou, *Nanotechnology*, 2010, **21**, 215701.
215 R. Houdré, J. L. Gibernon, P. Pellandini, R. P. Stanley, U. Oesterle, C. Weisbuch, J. O'Gorman, B. Roycroft and M. Ilegems, *Phys. Rev. B: Condens. Matter*, 1995, **52**, 7810.
216 D. Liu, W. H. Zhang, X. Zhu, L. Cao, B. S. Zou and Z. B. Zhang, *Mod. Phys. Lett. B*, 2007, **21**, 543.
217 D. W. Snoke, *Science*, 2002, **298**, 1368.
218 A. van Dijken, E. A. Meulenkamp, D. Vanmaekelbergh and A. Meijerink, *J. Lumin.*, 2000, **90**, 123.
219 J. M. Blatt, K. W. Böer and W. Brandt, *Phys. Rev.*, 1962, **126**, 1691.
220 L. V. Butov, C. W. Lai, A. L. Ivanov, A. C. Gossard and D. S. Chemla, *Nature*, 2002, **417**, 47.
221 J. Ni, H. Yan, A. C. Wang, Y. Yang, C. L. Stern, A. W. Metz, S. Jin, L. Wang, T. J. Marks, J. R. Ireland and C. R. Kannewurf, *J. Am. Chem. Soc.*, 2005, **127**, 5613.
222 J. Zhou, P. Fei, Y. D. Gu, W. J. Mai, Y. F. Gao, R. Yang, G. Bao and Z. L. Wang, *Nano Lett.*, 2008, **8**, 3973.
223 Y. R. Ryu, T. S. Lee, J. A. Lubguban, H. W. White, B. J. Kim, Y. S. Park and C. J. Youn, *Appl. Phys. Lett.*, 2006, **88**, 241108.
224 Y. Yang, Y. Q. Li, S. Y. Fu and H. M. Xiao, *J. Phys. Chem. C*, 2008, **112**, 10553.
225 S. H. K. Park, C. S. Hwang, M. Ryu, S. Yang, C. Byun, J. Shin, J. I. Lee, K. Lee, M. S. Oh and S. Im, *Adv. Mater.*, 2009, **21**, 678.
226 Y. I. Alivov, E. V. Kalinina, A. E. Cherenkov, D. C. Look, B. M. Ataev, A. K. Omaev, M. V. Chukichev and D. M. Bagnall, *Appl. Phys. Lett.*, 2003, **83**, 4719.
227 Y. I. Alivov, J. E. Van Nostrand, D. C. Look, M. V. Chukichev and B. M. Ataev, *Appl. Phys. Lett.*, 2003, **83**, 2943.
228 Q. X. Yu, B. Xu, Q. H. Wu, Y. Liao, G. Z. Wang, R. C. Fang, H. Y. Lee and C. T. Lee, *Appl. Phys. Lett.*, 2003, **83**, 4713.
229 D. J. Rogers, F. H. Teherani, A. Yasan, K. Minder, P. Kung and M. Razeghi, *Appl. Phys. Lett.*, 2006, **88**, 141918.
230 R. W. Chuang, R. X. Wu, L. W. Lai and C. T. Lee, *Appl. Phys. Lett.*, 2007, **91**, 231113.
231 M. K. Lee, C. L. Ho and P. C. Chen, *IEEE Photonics Technol. Lett.*, 2008, **20**, 252.
232 O. Lupan, T. Pauporte and B. Viana, *Adv. Mater.*, 2010, **22**, 3298.
233 J. R. Sadaf, M. Q. Israr, S. Kishwar, O. Nur and M. Willander, *Nanoscale Res. Lett.*, 2010, **5**, 957.
234 J. B. You, X. W. Zhang, S. G. Zhang, J. X. Wang, Z. G. Yin, H. R. Tan, W. J. Zhang, P. K. Chu, B. Cui, A. M. Wowchak, A. M. Dabiran and P. P. Chow, *Appl. Phys. Lett.*, 2010, **96**, 201102.
235 R. Konenkamp, R. C. Word and M. Godinez, *Nano Lett.*, 2005, **5**, 2005.
236 X. W. Sun, J. Z. Huang, J. X. Wang and Z. Xu, *Nano Lett.*, 2008, **8**, 1219.
237 O. Lupan, T. Pauporte and B. Viana, *J. Phys. Chem. C*, 2010, **114**, 14781.
238 A. Tsukazaki, M. Kubota, A. Ohtomo, T. Onuma, K. Ohtani, H. Ohno, S. F. Chichibu and M. Kawasaki, *Jpn. J. Appl. Phys.*, 2005, **44**, L643.
239 S. J. Jiao, Z. Z. Zhang, Y. M. Lu, D. Z. Shen, B. Yao, J. Y. Zhang, B. H. Li, D. X. Zhao, X. W. Fan and Z. K. Tang, *Appl. Phys. Lett.*, 2006, **88**, 031911.
240 J. H. Lim, C. K. Kang, K. K. Kim, I. K. Park, D. K. Hwang and S. J. Park, *Adv. Mater.*, 2006, **18**, 2720.
241 W. Liu, S. L. Gu, J. D. Ye, S. M. Zhu, S. M. Liu, X. Zhou, R. Zhang, Y. Shi, Y. D. Zheng, Y. Hang and C. L. Zhang, *Appl. Phys. Lett.*, 2006, **88**, 092101.
242 W. Z. Xu, Z. Z. Ye, Y. J. Zeng, L. P. Zhu, B. H. Zhao, L. Jiang, J. G. Lu, H. P. He and S. B. Zhang, *Appl. Phys. Lett.*, 2006, **88**, 173506.
243 Z. P. Wei, Y. M. Lu, D. Z. Shen, Z. Z. Zhang, B. Yao, B. H. Li, J. Y. Zhang, D. X. Zhao, X. W. Fan and Z. K. Tang, *Appl. Phys. Lett.*, 2007, **90**, 042113.
244 K. Nakahara, S. Akasaka, H. Yuji, K. Tamura, T. Fujii, Y. Nishimoto, D. Takamizu, A. Sasaki, T. Tanabe, H. Takasu, H. Amaike, T. Onuma, S. F. Chichibu, A. Tsukazaki, A. Ohtomo and M. Kawasaki, *Appl. Phys. Lett.*, 2010, **97**, 013501.
245 D. K. Hwang, S. H. Kang, J. H. Lim, E. J. Yang, J. Y. Oh, J. H. Yang and S. J. Park, *Appl. Phys. Lett.*, 2005, **86**, 222101.
246 H. C. Chen, M. J. Chen, Y. C. Cheng, J. R. Yang and M. Shiojiri, *IEEE Photonics Technol. Lett.*, 2010, **22**, 248.
247 Z. Guo, D. X. Zhao, Y. C. Liu, D. Z. Shen, B. Yao, Z. Z. Zhang and B. H. Li, *J. Phys. Chem. C*, 2010, **114**, 15499.
248 X. Y. Ma, J. W. Pan, P. L. Chen, D. S. Li, H. Zhang, Y. Yang and D. R. Yang, *Opt. Express*, 2009, **17**, 14426.
249 J. Y. Zhang, Q. F. Zhang, T. S. Deng and J. L. Wu, *Appl. Phys. Lett.*, 2009, **95**, 211107.
250 S. Chu, M. Olmedo, Z. Yang, J. Y. Kong and J. L. Liu, *Appl. Phys. Lett.*, 2008, **93**, 181106.
251 X. Y. Ma, P. L. Chen, D. S. Li, Y. Y. Zhang and D. R. Yang, *Appl. Phys. Lett.*, 2007, **91**, 251109.
252 R. F. Oulton, V. J. Sorger, T. Zentgraf, R.-M. Ma, C. Gladden, L. Dai, G. Bartal and X. Zhang, *Nature*, 2009, **461**, 629.
253 M. A. Noginov, G. Zhu, A. M. Belgrave, R. Bakker, V. M. Shalaev, E. E. Narimanov, S. Stout, E. Herz, T. Suteewong and U. Wiesner, *Nature*, 2009, **460**, 1110.
254 C. Z. Ning, *Phys. Status Solidi B*, 2010, **247**, 774.
255 V. G. Bordo, *Phys. Rev. B: Condens. Matter Mater. Phys.*, 2010, **81**, 035420.
256 R. Yan, D. Gargas and P. Yang, *Nat. Photonics*, 2009, **3**, 569.
257 C. G. Van de Walle and J. Neugebauer, *Nature*, 2003, **423**, 626.
258 V. Avrutin, D. J. Silversmith and H. Morkoç, *Proc. IEEE*, 2010, **98**, 1269.
259 P. Yang, R. Yan and M. Fardy, *Nano Lett.*, 2010, **10**, 1529.
260 D. J. Bergman and M. I. Stockman, *Phys. Rev. Lett.*, 2003, **90**, 027402.

